Cabazitaxel-loaded poly(alkyl cyanoacrylate) nanoparticles: Toxicity and changes in the proteome of breast, colon and prostate cancer cells

Anders Øverbye[a], Maria Lyngaas Torgersen[a], Tonje Sønstevold[a,b], Tore Geir Iversen[a], Ýrr Mørch[c], Tore Skotland[a], and Kirsten Sandvig[a,b,*]

[a] Department of Molecular Cell Biology, Institute for Cancer Research, Oslo University Hospital, The Norwegian Radium Hospital, Oslo, Norway

[b] Department of Biosciences, University of Oslo, Oslo, Norway

[c] Department of Biotechnology and Nanomedicine, SINTEF AS, Trondheim, Norway

* Communicating author: ksandvig@radium.uio.no

Number of words in the main text: 6058

Number of words in the abstract: 238

Figures: 9

Tables: 2

References: 67

Supplementary: 7 figures and 1 table

Keywords: nanoparticles; poly(alkyl cyanoacrylate); cabazitaxel; proteomics; cancer

ABSTRACT

Nanoparticles composed of poly(alkyl cyanoacrylate) (PACA) have shown great promise due to their biodegradability and high drug loading capacity. Development of optimal PACA nanocarriers requires detailed analysis of the overall cellular impact exerted by PACA variants. We here perform a comprehensive comparison of cabazitaxel (CBZ)-loaded nanocarriers composed of three different PACA monomers, i.e. poly(n-butyl cyanoacrylate) (PBCA), poly(2-ethylbutyl cyanoacrylate) (PEBCA) and poly(octyl cyanoacrylate) (POCA). The cytotoxicity of drug-loaded and empty PACA nanoparticles were compared to that of free CBZ across a panel of nine cancer cell lines by assessing cellular metabolism, proliferation and protein synthesis. The analyses revealed that the cytotoxicity of all CBZ-loaded PACAs was similar to that of free CBZ for all cell lines tested, whereas the empty PACAs exerted much lower toxicity. To increase our understanding of the toxic effects of these treatments comprehensive MS-based proteomics were performed with HCT116, MDA-MB-231 and PC3 cells incubated with PACA-CBZ variants or free CBZ. Interestingly, PACA-CBZ specifically led to decreased levels of proteins involved in focal adhesion and stress fibers in all cell lines. Since we recently demonstrated that encapsulation of CBZ within PEBCA nanoparticles significantly improved the therapeutic effect of CBZ on a patient derived xenograft model in mice, we investigated the effects of this PACA variant more closely by immunoblotting. Interestingly, we detected several changes in the protein expression and degree of phosphorylation of SRC-pathway proteins that can be relevant for the therapeutic effects of these substances.

Introduction

Many studies now focus on using drug-loaded nanoparticles (NPs) to enhance the therapeutic effect and reduce the side effects of drugs given to cancer patients. Different NPs carrying a wide variety of drugs have been designed and tested (Mallick and Choi 2014; Shi et al. 2017; Taurin et al. 2012; Torchilin 2014). Among these, NPs composed of poly(alkyl cyanoacrylate), PACAs, have shown great promise due to their biodegradability and high loading capacity (Aslund et al. 2017; Sulheim et al. 2016; Vauthier et al. 2003). Early screening of toxic effects of NPs is important for development of the product, and to keep costs as low as possible. This screening is most often performed by using standardized assays to test the toxic effect on cancer-derived cell lines. However, different results are obtained depending on the test system and cell line used, and the reasons behind the differences are most often not understood (Szwed et al. 2019). Knowledge about the mechanism for NP entry into cells, the subsequent intracellular transport and the effect on cells are important to develop an optimal composition of the NPs. For detailed analysis of the overall molecular impact on cells treated with NPs, mass spectrometry (MS) proteomic analysis can be useful, as this enables identification and quantification of proteins affected, and subsequent information about the molecular machinery, cellular processes and biological compartments involved.

Cytotoxic drugs of the taxane-class have been used in cancer treatment for decades with good results (Baciarello et al. 2018). However, various side-effects and acquired resistance may result in discontinuation of the treatment. Encapsulation of the drug into NPs may reduce the systemic exposure and thus the unwanted toxic effects. Furthermore, such encapsulation may result in a different biodistribution, and a higher tumor uptake due to increased circulation times of the drug-containing NPs (Fusser et al. 2019) and the enhanced permeability and retention (EPR) effect (Kim et al. 2017; Matsumura and Maeda 1986;

Ruoslahti et al. 2010). However, how NPs are transported over the endothelial cell layer is still being discussed (Sindhwani et al. 2020; Skotland and Sandvig 2021). The therapeutic taxane drugs include paclitaxel (PTX), docetaxel (DTX) and more recently also cabazitaxel (CBZ). CBZ was approved by the US Food and Drug Administration (FDA) in 2010 for treatment of refractory prostate cancer as a second line drug after DTX chemotherapy (Mita et al. 2012; Paller and Antonarakis 2011). One advantage of CBZ is its low affinity for the P-glycoprotein, which can transfer drugs out of cells; use of CBZ will therefore reduce the possibility of obtaining drug resistance (Duran et al. 2018; Machioka et al. 2018; Vrignaud et al. 2013). The poor water solubility of taxanes complicates administration of the free drug. However, improved compatibility and solubility of CBZ in alkyl cyanoacrylate monomer solution allow for encapsulation of high concentrations of CBZ in PACA NPs (Aslund et al. 2017).

We have previously shown that CBZ-loaded poly(2-ethylbutyl cyanoacrylate) (PEBCA) NPs had a better therapeutic effect on the tumor than free CBZ and that the increased efficacy obtained with these NPs partly may be due to infiltration of more M1 (anti-tumorigenic) than M2 (pro-tumorigenic) macrophages in the tumor (Fusser et al. 2019) investigated several cancer cell lines for their response to three variants of PACA NPs, i.e. PEBCA, poly(n-butyl cyanoacrylate) (PBCA) and poly(octyl cyanoacrylate) (POCA) (Sulheim et al. 2017; Szwed et al. 2019; Sønstevold et al. 2020). As recently reported, the toxic effects of these NPs were cell type dependent, and surprisingly these very similar NPs were shown to induce different death mechanisms (Szwed et al. 2019). To improve cancer therapy, we need to unravel the intoxication mechanisms of the drugs used, and the aim of the current study was to investigate the toxic effect of the three CBZ-containing PACA NPs with free CBZ and the empty PACA NPs. We here report the cytotoxicity obtained using these three PACAs with encapsulated CBZ, i.e. PBCA-CBZ, PEBCA-CBZ and POCA-CBZ, and

compare the toxicity with that obtained using either free CBZ or these PACAs without encapsulated drug across a panel of nine cell lines, i.e. MDA-MB-231, SKBR3, MDA-MB-468, MCF-7, HT29, HCT116, PC3, LNCaP and HeLa. Thus, we have here studied four breast cancer cell lines, two colon cancer cell lines and two prostate cancer cell lines, as well as the very commonly used HeLa cervical cancer cell line. To elucidate mechanisms of intoxication detailed MS proteomic analyses of HCT116, PC3 and MDA-MB-231 cells (i.e. one colon, prostate and breast cancer cell line) treated with these substances revealed several changes in protein expression and show, together with Western blotting analyses, important changes in the expression and phosphorylation of SRC-pathway proteins that may be related to therapeutic effects.

Materials and methods

Synthesis of NPs

PACA NPs were prepared using the miniemulsion polymerization method as previously described (Fusser et al. 2019; Sulheim et al. 2017; Szwed et al. 2019). Briefly, PBCA, PEBCA, or POCA NPs were made by mixing an oil phase consisting of the monomers butyl-, ethylbutyl-, or octyl cyanoacrylate (0.45 g, Cuantum Medical Cosmetics, Spain and Henkel Loctite, Ireland), a neutral oil (Miglyol® 812, 2% (w/w), Cremer, USA) and vanillin (6% (w/w), Sigma-Aldrich, USA with an aqueous phase consisting of hydrochloric acid (0.1 M, 5 ml) and the PEG-surfactants Kolliphor® HS15 (4 mM, Sigma-Aldrich) and Pluronic® F68 (1 mM, Sigma-Aldrich). Particles containing cytostatic drug were prepared by adding CBZ or DTX (10% (w/w), Biochempartner Co. Ltd., China) to the oil phase. The oil in water miniemulsion was made using a tip sonifier (Branson, 60% amplitude, 6x30 sec with 10 sec pauses, on ice). The polymerization was carried out at room temperature overnight on rotation. The pH was increased to pH 5.0 using 0.1 M NaOH and the polymerization

continued for 5 h on rotation. The dispersion was extensively dialyzed (Spectra/ Por dialysis membrane MWCO 100,000 Da, Spectrum Labs, USA) against 1 mM HCl (pH 3.0) to remove excess PEG surfactants (Morch et al. 2015). The NPs are stable for at least 12 months when stored in a refrigerator in this solution. We have previously shown that cytotoxic effects of PACA NPs are dependent on the type of monomer and independent of the type of PEG used (Sulheim et al. 2017). These PACA NPs are stable for at least 24 h in complete growth medium containing 10% fetal calf serum (Szwed et al. 2019).

Characterization of NPs

The size (diameter; z-average), polydispersity index (PDI) and the zeta potential of the NPs were measured by dynamic light scattering and laser Doppler Micro-electrophoresis using a Zetasizer Nano ZS (Malvern Instruments, UK). To calculate the amount of encapsulated drug, the drug was extracted from the particles by diluting 10x in acetone and quantified by liquid chromatography coupled to MS (LC-MS/MS) as earlier described (Fusser et al. 2019).

Cell lines

Several different commonly used cancer cell lines were used. The MDA-MB-231, (triple negative breast cancer, Claudin low), and LNCaP (prostate cancer, AR-responsive) were cultured in RPMI 1640; the MDA-MB-468 (triple negative breast cancer, basal), HeLa (cervical cancer), HT29 (colorectal cancer, *p53*mut), HCT116 (colorectal cancer *p53*wt; aggressive type of colon carcinoma), SKBR3 (breast cancer, HER2+), PC3 (prostate cancer, AR-resistant) and the MCF-7 (breast cancer, luminal A) cell lines were cultured in DMEM. The medium was fortified with 10% (w/v) fetal calf serum (Sigma-Aldrich) and 100 units/ml penicillin/streptomycin (PenStrep®, Sigma-Aldrich). All cell lines were obtained from ATCC and were routinely tested for mycoplasma.

Cytotoxicity studies

Cells growing in 24- or 96-well plates in an atmosphere of 5% (v/v) CO_2 were incubated with serial dilutions of PBCA-CBZ, POCA-CBZ, PEBCA-CBZ, CBZ (non-encapsulated CBZ) dissolved in Tween-80 (Fluka), and the same PACAs without CBZ for different periods of time as detailed below and in the figure legends. Toxicity was assessed either by the commonly used MTT (4,5-dimethylthiazol-2-yl)-2,5-diphenyltetrazolium bromide) test, by measuring cell proliferation based on [^{3}H]thymidine incorporation, or by measuring protein synthesis by incorporation of [^{3}H]leucine.

MTT test

Although the MTT test is commonly used as a "cell viability test", it is now known that this test measures the rate of the glycolytic NAD(P)H production (Stockert et al. 2018). When using the MTT test, theThe cells were incubated with the different NPs or substances at 37 °C for 72 h if not stated otherwise. The initial cell density was 5,000 or 8,000 cells per well in a 96-well plate. For the temperature effect studies the substances were incubated with cells for 2 h at 4, 22 and 37 °C, washed twice with complete medium and then incubated at 37 °C for 70 h. For pulse-chase studies cells were incubated with the substances at 37 °C for 5, 15, 30, 60 and 120 min, washed twice with complete medium before continuing the incubation at 37 °C for a total of 72 h. Following such incubations, the cell medium was aspirated and exchanged with 100 µl of medium containing a final concentration of 250 µg MTT/ml. The incubation was continued for 3 h at 37 °C for formation of the formazan-particles, which were subsequently dissolved in DMSO with 1% (w/v) NH_4Cl during vigorous shaking for 10 min. The absorbance was read in a plate reader (Biosys Ltd., Essex, UK) at 570 nm, and background from absorbance at 650 nm was subtracted.

Cell proliferation measured by [^{3}H]thymidine incorporation

Incorporation of [^{3}H]thymidine into DNA was used to estimate cell proliferation. The cells were incubated at 37 °C for 24 h with the different NPs or other substances, in a 24-well plate with an initial cell density of 40,000-60,000 per well. The cell medium was then aspirated and substituted with serum free cell medium containing [^{3}H]thymidine (3 μg/ml; 75 μCi/ml). The incubation was continued for 30 min at 37 °C. The medium was removed and 5% (w/v) trichloroacetic acid (TCA) was added. After 5 min the cells were washed twice with TCA and solubilized with 200 μl of 0.1M KOH, before mixing with 3 ml scintillation fluid (Perkin Elmer, USA). The radioactivity was counted for 1 min in a scintillation counter (Tri-Carb 2100TR, Packard Bioscience, USA).

Protein synthesis measured by [^{3}H]leucine incorporation

To determine the impact of PEBCA-CBZ and CBZ on protein synthesis, the cells were incubated with these substances at 37 °C for 24 h in a 24 well plate with an initial cell density of 40,000-60,000 per well. The cell medium was then aspirated, the cells washed once with leucine-free HEPES medium (28 mM HEPES, (4-(2-hydroxyethyl)-1-piperazineethanesulfonic acid) in MEM) and further incubated with leucine-free HEPES medium containing [^{3}H]leucine (2 μCi/ml) for 30 min at 37 °C. The medium was removed and 5% (w/v) TCA was added to precipitate proteins and thereby permeabilize the cells. After 5 min the cells were washed again with 5% (w/v) TCA and solubilized with 200 μl of 0.1M KOH, before mixing with 3 ml scintillation fluid and counting the radioactivity as described above.

LC-MS/MS analyses

Mass spectrometric-based proteomic analyses were performed using HCT116, MDA-MB-231 or PC3 cells following treatment of the cells with CBZ or PACA-CBZ in 6-well plates (100,000 cells/well for HCT116, and 150,000 cells/well for PC3 and MDA-MB-231). Cells were incubated for 24 hr after seeding to ensure adherence and then treated with either 3 or 10 nM free CBZ, PBCA-CBZ, PEBCA-CBZ or POCA-CBZ. Control samples were prepared using either untreated cells or cells treated with 2.7 µg/ml empty PEBCA. After treatment for 24 h the cells were washed with 10 mM phosphate buffered saline (PBS; containing 140 mM NaCl) and kept on ice. Cellular proteins were precipitated by methanol/chloroform/water (4/1/3). After removing the supernatant, the protein pellet was reconstituted in 50 mM ammonium bicarbonate, pH 8.0. Next, the proteins were treated with a reducing agent, 25 mM of dithiothreitol (DTT; Sigma-Aldrich), and then alkylated using 65 mM of iodoacetamide (Sigma-Aldrich). Finally, proteins were digested overnight at 37 °C using 3.75 ng/µl trypsin (Promega; sequencing grade). The peptides were desalted using an in-house C_{18} StageTip; each StageTip was made with three layers of C_{18} Empore Extraction disks (Varian, St. Paul, USA). The obtained peptides were dried in a vacuum concentrator and then resuspended in 7 µl 0.1% (v/v) formic acid.

LC-MS/MS analysis was performed on an Orbitrap QExactive Plus mass spectrometer operated in the data-dependent mode to switch automatically between MS and MS/MS acquisition. Survey full-scan MS spectra (*m*/*z* 400-1200) were acquired in Orbitrap with a mass resolution of 70,000 at *m*/*z* 200. The automatic gain control (AGC) target was set to 3,000,000, and the maximum injection time was 100 ms. MS/MS spectra were acquired of the ten most abundant ions (Top10 method) with a dynamic exclusion time of 30 sec. The AGC target was set to 150,000, and the isolation window was 2 *m*/*z*. Ions with charge states 2+, 3+, and 4+ were sequentially fragmented by higher energy collisional

dissociation (HCD) with a normalized collision energy (NCE) of 25%, fixed first mass was set at 100. In all cases, one microscan was recorded using dynamic exclusion of 30 s.

Raw files were transferred to MaxQuant v 1.5.7.4 (Cox and Mann 2008), mapping the spectra over human canonical proteome including all isoforms (Uniprot version 03.2017). The mass tolerance for MaxQuant was 20 ppm for peptides and 4.5 ppm for fragment ions. To determine post-translational modifications, a neutral loss scan for 80 m/z was performed on MS2 for phosphorylation of Ser, Thr or Tyr, while Leu-Arg-Gly-Gly-tetrapeptide and/or Gly-Gly dipeptide from ubiquitin bound to Lys was investigated for ubiquitylation modification (Peng et al. 2003). Total ubiquitylation was measured by depth loss scan of RPS27A (pseudogene UBA) protein expression, including a minimum threshold of three peptides. For comparative proteomics analysis of treated and control cells, only those protein groups that had 100% identification in at least one group were considered. False discovery rate of protein discovery was less than 0.01 as determined by reverse decoy search (Keich et al. 2018).

Gene Ontology (GO) term enrichment was used to classify proteins changed after treatment. GO is a technique for interpreting sets of genes making use of the Gene Ontology system of classification, in which genes are assigned to a set of predefined bins depending on their functional characteristics (Gaudet and Dessimoz 2017).

Immunoblotting

Cell lysates were made by washing the treated cells with cold PBS and lysis in 1.1x Laemmli sample buffer. The lysate was boiled, sonicated briefly to reduce viscosity, and the protein concentration was measured by BCA assay (Thermo Scientific, Waltham, MA). Reducing agent (50 mM DTT) was added after protein determination. Equal amounts of protein were loaded to the gel and separated using 4–20% SDS-PAGE. The proteins were then transferred to a PVDF membrane, which was blocked by drying and incubated overnight with the

primary antibodies in 5% BSA, followed by incubation for 35 min with HRP-conjugated secondary antibodies. Detection was performed using SuperSignal West Dura Extended Duration Substrate (Thermo Scientific, Waltham, MA) in a ChemiDoc Imaging System (Bio-Rad Laboratories, Hercules, CA). Quantification of the signal intensities were performed using the Quantity One software (Bio-Rad Laboratories, Hercules, CA) and the signals were normalized to the loading control. The following antibodies were used: LAMP1, LAMP2a, PTPB1, BCAR1, and CDCK1 were from Cell Signaling Technologies, whereas SRC and CSK were from Sigma-Aldrich.

Results and discussion

Characterization of NPs

The size distributions of the PACA NPs without drug and the drug-loaded PACAs are shown in Figure 1, and the mean size, polydispersity index (PDI) and the zeta potential for all preparations studied are listed in Table 1. As can be seen, the diameter of the various PACAs increased somewhat in size following encapsulation of CBZ (diameters of 129-153 nm for PACAs and 181-209 nm for CBZ-loaded PACAs), whereas the PDI and the zeta potential were very similar (slightly negative) for empty PACAs and CBZ-loaded PACAs.

Cell toxicity following incubation of cells with the NPs

Analysis of the cytotoxicity of CBZ-loaded PACAs, empty PACAs and free CBZ was performed using the MTT assay following 72 h incubation of the substances with the nine different cell lines (MDA-MB-231, SKBR3, MDA-MB-468, MCF-7, HT29, HCT116, PC3, LNCaP and HeLa). These analyses revealed that PACAs containing CBZ were much more toxic to cells than the empty PACAs and that the toxicity of all CBZ-loaded PACAs was similar to that of free CBZ for all cell lines tested (Figure 2). The empty NPs gave a 100- to

1000-fold less toxic effect than the CBZ-loaded NPs, and the empty NPs showed a similar cell-type dependent cytotoxic profile as recently reported (Szwed et al. 2019).

The effect of these substances on cell proliferation (incorporation of [^{3}H]thymidine) and protein synthesis (incorporation of [^{3}H]leucine) following incubations for 24 h revealed similar patterns (Supplementary Figure 1) as those described above when using the MTT assay after 72 h incubation. The MTT assay was performed following 72 h incubation as we have earlier shown with PEBCA NPs and lipid nanocapsules (Fusser et al. 2019; Szwed et al. 2020). that 24 and 48 h incubation give much smaller effects with this assay. We find it useful to include measurements of cell proliferation (incorporation of [^{3}H]thymidine) and protein synthesis (incorporation of [^{3}H]leucine) in such analyses as these tests may give important information different from that obtained with the MTT test. Specifically, protein synthesis in cells is sensitive to changes in ion composition, pH, ER stress and signaling (Cahn and Lubin 1978; Hetz 2012; Pakos-Zebrucka et al. 2016) and can provide an early readout of toxic effects.

Also, morphological studies of the colorectal cells HCT116 and the breast cancer triple-negative cells MDA-MB-231 (i.e. two cell lines showing different responses to these substances in Figure 2) did not reveal any large differences in response to the free CBZ or CBZ-loaded PEBCA; micrographs of HCT116 cells are shown in Supplementary Figure 2; micrographs of MDA-MB-231 cells are not shown.

Next, we exposed cells to the various PACA formulations for different times and looked for differences in long term effects, as this may be of importance in an *in vivo* situation where cells or tissues are exposed to drug-loaded NPs for a given time. To this end, HCT116 and MDA-MB-231 cells were first incubated with free CBZ, PEBCA-CBZ and PEBCA at 4, 22 or 37 °C for 2 h followed by washing of cells, further incubation for 70 h at 37 °C, and then measuring cell viability using the MTT assay. As shown in Supplementary Figure 3 only

small differences were observed between free CBZ and PEBCA-CBZ under these conditions, and the empty NPs either had a low or negligible toxic effect. Importantly, these data demonstrated that the NPs do not to any significant effect stick to the cells as only little toxicity is observed after pre-incubation at 4 °C. Similarly, no effect was seen after preincubation of PBCA-CBZ or POCA-CBZ with these cells at 4 °C and the same holds true for all these NPs when using HT29 cells (data not shown).

These results make it possible to investigate the uptake kinetics of the various NP formulations by performing pulse-chase studies. HT29 cells were incubated with the different substances for 5 min to 120 min, then the cells were washed, and the incubations continued for a total of 72 h before cytotoxicity was measured. Interestingly, the results reveal both different kinetics and degree of toxicity with the various substances, with POCA-CBZ being most toxic and PEBCA-CBZ being least toxic when the substances were allowed to internalize for only 15-120 min (Figure 3), in contrast to the observations after 72 h of continuous incubation where all CBZ-loaded PACAs and free CBZ were equally toxic (Figure 3). These differences may be of importance following intravenous injection of the drug-loaded NPs as cells or tissues may be exposed to the NPs only for a short time.

Since CBZ is considered an improvement over docetaxel (DTX) but is yet only administered in castrate-resistant prostate cancer during DTX-resistance (Paller and Antonarakis 2011), we tested whether CBZ showed similar or improved toxicological profile than DTX when incorporated into PACA NPs. For all cell lines tested, free CBZ gave a similar or stronger toxic effect than free DTX, and PEBCA-CBZ was more toxic than PEBCA-DTX in the breast cancer cell lines MDA-MB-231, MDA-MB-468 and SKBR3. PEBCA-CBZ also gave a stronger toxic effect than PEBCA-DTX at high drug concentrations in PC3 and LNCaP cells, i.e. in both prostate cancer cell lines tested (Supplementary Figure 4).

MS analyses of the proteomes

To investigate the molecular mechanisms affected during interactions of cells with CBZ-containing PACAs, free CBZ and empty PACAs, we analyzed which proteins were up-regulated or down-regulated in response to treatment of cells with the different substances. Such changes were studied using comprehensive MS-based proteomics with HCT116, MDA-MB-231 and PC3 cells. We have previously demonstrated that the uptake of the three PACA NPs occurs to a similar extent in each of these cell lines (Szwed et al. 2019).

Most of these analyses were performed using the HCT116 cells, which were treated for 24 h with two doses of free CBZ and the CBZ-containing PACAs; 3 and 10 nM CBZ were used, i.e. the concentrations giving approximately 30% and 50% reduction in cell proliferation and protein synthesis (Supplementary Figure 1). The proteomes obtained from treated cells were compared to the proteomes obtained from untreated cells and normalized against cells incubated with a concentration of empty NPs corresponding to the NP concentration used when cells were incubated with CBZ-loaded NPs (0.4-0.7 µg/ml). The results from analyses with the low concentration of empty PACAs were indistinguishable from untreated cells and were merged with the results from untreated controls to increase statistical power.

The MS label-free quantification of HCT116 revealed 2617 proteins detected in 2 out of 3 technical replicates, with 2 or more peptides or 1 high quality peptide spectrum (minimum peptide spectrum score of 15.0). The number of proteins with significantly ($p<0.01$) changed protein levels were in the range 209-217 for CBZ-loaded PACAs and 278 for cells treated with free CBZ (Figure 4A). Thus, more proteins were altered following treatment with free CBZ than with CBZ-loaded PACAs. Qualitatively, 12% more proteins displayed a reduced than an enriched expression after treatment with CBZ and CBZ-loaded PACAs (Figure 4B). Increasing the concentration of CBZ resulted in 21% more proteins

showing increased differences in the protein expression as displayed in the volcano plots (Supplementary Figure 5).

To study the effect of a treatment on a cellular level for all proteins, it is often useful to display the enriched proteins in a network of interaction partners. Such network analysis tools (i.e. String) will also investigate and sort groups of protein connections and their relative enrichment in one or more Gene Ontology (GO) groups (biological process, molecular function, cellular component), and thus indicate which cellular processes a treatment affect (Ashburner et al. 2000).

The proteomic data were used to address the five scenarios listed in Table 2. When comparing all cells treated with CBZ disregarding NP (Scenario 1 in Table 2; see also Supplementary Figure 6), a small subset of 15 proteins was detected as increased, creating a network (Figure 5A). Prominent among these proteins were members of the methylosome, a large protein complex involved in methylation of arginine (Friesen et al. 2002), (labeled green in the figure, e.g. WDR77 and SNRPF). A subset of the proteins was not detected in control cells at all - including MARCKSL1 (controls cell movement by regulating the actin cytoskeleton homeostasis and filopodium and lamellipodium formation) (Bjorkblom et al. 2012), YTHDF3 (methyladenosine RNA binding protein) (Awakura et al. 2008) and UCHL5 (ubiquitin C-terminal hydrolase, and a positive cancer prognosis marker) (Arpalahti et al. 2017; Chadchankar et al. 2019) while WDR77 showed a 9-fold increase in abundance in treated cells.

As shown in Figure 5B (and Supplementary Table 1) enriched proteins showed a prevalence for nuclear lumen localization (labelled in blue), while two annexin-proteins were also detected. The annexin protein family is involved in inhibition (regulation) of phospholipases (labelled in red) in addition to other cellular functions (Buckland and Wilton 1998; Tcatchoff et al. 2012).

Treatment with CBZ or CBZ-loaded PACAs also led to decreased amounts of proteins (Figure 5C-D, Supplementary Table 1), such as ribonuclear (labelled green in the figure) and translational and focal adhesion proteins (labeled red in the figure), and dendrite (structural proteins; labelled blue), reflecting the role of CBZ as an inhibitor of microtubule disruption, thereby affecting cellular shape, cell division and external communication (Sapega et al. 2018; Smiyun et al. 2017). Interestingly, a very profound reduction in LAMP1 (lysosomal-associated membrane protein 1), which was reduced to 7% of the control level (Figure 5C), might suggest that the CBZ treatment results in fewer lysosomes. We followed up this observation by performing Western blot analyses of the lysosomal markers LAMP1, LAMP2a and cathepsin D following incubation of HCT116 cells with 10 nM CBZ or 10 nM PEBCA-CBZ for 0.25 - 24 h. As shown in Supplementary Figure 7A-B, the decrease in LAMP1 was then less pronounced, i.e. down to 70% of control; we speculate if the different decrease obtained for LAMP1 by these methods is due to LAMP1 being a membrane-associated glycoprotein that may result in less LAMP1-originating peptides being detected by the MS analyses or sensitivity of the dynamic range of the two different protein quantification methods used. The immunoblotting analysis revealed a decrease also for LAMP2a as a function of incubation time, although not as large as for LAMP1, whereas no significant changes were observed for cathepsin D.

Proteomic analyses of HCT116 cells treated with increasing concentrations (3 and 10 nM) of CBZ (Scenario 2 in Table 2) gave up-regulation of proteins (Figure 6A-B, Supplementary Table 1) involved in ketone catabolism, glycolysis (labeled red in the figure) and cytoskeleton organization (labeled blue in the figure), i.e. in processes involved in initiating decreased cellular viability. A majority of the enriched proteins were involved in ribonuclear assembly (labeled green). Noteworthy, is also the increase in isoforms of beta-tubulin (TUBB2a, TUBB4b, TUBB3a and TUBB8), which indicates that newly synthesized

tubulin is formed to address the increase in microtubule stabilization caused by the highest dose of CBZ. On the other side, higher concentrations of CBZ resulted in reduced levels of proteins (Figure 6C-D, Supplementary Table 1) known to be involved in cell division and translation (labelled in green and blue) and in general an apparent larger transcriptional regulation. In particular the absence of KRAS (grey in Figure 6C; or its undistinguishable homologues NRAS/HRAS) after increased CBZ is interesting as RAS is an important oncogene and driver of the Raf/ERK-cascade (Santos and Crespo 2018). A subset of the depleted proteins has a role in ER/ribosome functions, indicative of general reduction in protein production (labelled red and orange).

A comparison of the effect of free CBZ to all CBZ-loaded PACAs in HCT116 cells (Scenario 3 in Table 2) displayed that CBZ-loaded PACAs gave the strongest increase in two distinct protein complexes (Figure 7A-B; Supplementary Table 1). There was an increase in core components of the spliceosome (labeled blue in the figure) that has been linked to differential increase in expression of proteins with lower ATP spending (Agafonov et al. 2011; Will and Luhrmann 2011). Also there was an increase in the Rho signal complex (labeled red in the figure), with the associated member TAX1-binding protein 3 (TAX1BP3) which increased 4-fold, and is involved in regulating interactions with several pathways, Wnt in particular (Florian et al. 2013; Iwai et al. 2010; Lechel and Rudolph 2008), which also showed increased expression. XPC (in orange) is acting as damage sensing and DNA-binding factor (Clement et al. 2011). Nuclear localization was a predominant feature for the enriched proteins (labelled green). Down-regulation of proteins in cells treated with CBZ-loaded PACAs compared to cells treated with free CBZ (Figure 7C-D, Supplementary Table 1) includes proteins related to the stress fibers (labeled green in the figure), such as ezrin (EZR), zyxin (ZYX) and paxillin (PXN). Stress fibers and focal adhesions proteins are categorized as proteins involved in response to membrane events and change in cell topology and

mechanical tension (Burridge and Guilluy 2016). Furthermore, the key signaling tyrosine kinase SRC was reduced by 33% (shown below to be reduced by 28% in western blotting analyses). Additionally, translational termination is more prominent (proteins labeled red in the figure), indicating a difference at the transcription level as well. In sum, the changes induced in HCT116 cells by encapsulating CBZ in PACAs mainly relate to cellular structural organization, indicated by the difference in expression levels of proteins related to Rho regulation for free CBZ, and changes in the focal adhesion complex for CBZ-loaded PACAs. Several proteins were found to be involved in RNA processing, including a subset of ribosomal proteins (labeled blue). A comparison of the proteome changes after treatment with increased concentration of free CBZ and PACA-CBZ indicated that the latter treatment has a larger impact on protein change (Volcano plots in Supplementary Fig. 5), although the number of proteins changed was higher in cells treated with CBZ than in cells treated with PACA-CBZ (Figure 4).

We also compared the effect on expression of various proteins in HCT116 cells following treatment of these cells with the various PACA NPs (Scenario 4 in Table 2), but only minor differences were then obtained (data not shown). Thus, if there are differences in the proteome of the HCT116 cells due to treatment with the various PACAs, such differences are hidden by the larger changes obtained due to the presence of CBZ. To address possible cell-specific effects of CBZ-loaded PACAs, proteomic analysis was performed also using the breast cancer cell line MDA-MB-231 and the prostate cancer cell line PC3 (Scenario 5 in Table 2). However, the CBZ-loaded PACAs did not give any significant different changes in the proteome of these cell lines (data not shown).

Since PEBCA-CBZ recently was shown to give a much better therapeutic effect than free CBZ on a patient derived xenograft model in mice (Fusser et al. 2019), we decided to look more closely into a comparison of PEBCA-CBZ with free CBZ (using the very similar

data obtained with low dose PEBCA and untreated cells as controls). The resulting proteomic analyses reveal cell specific proteomes with 33% overlap between proteins being changed in HCT116, MDA-MB-231 and PC3 cells (Figure 8A); these data were comparable to the 36% overlap of data reported for transcriptomes (MERAV database, http://merav.wit.edu, (Shaul et al. 2016) of these cell lines (shown for comparison in Figure 8B). The proteins detected in these three cell lines were then analyzed with focus on differences between cells treated with PEBCA-CBZ versus free CBZ. These analyses revealed decreased levels of protein involved in focal adhesion and stress fibers in all cell lines (Supplementary Table 1). Importantly, the most striking differences was observed in the levels and post translational modification of proteins in the SRC-signaling pathway (Figure 9 and Supplementary Table 1), and we therefore decided to look more into changes of proteins involved in SRC signaling by using Western blot analyses.

SRC-pathway proteins

Immunoblotting analyses of the SRC-pathway proteins (Figure 9), i.e. SRC, CSK (C-terminal SRC kinase), BCAR1 (Breast cancer anti-estrogen protein 1; also called p130cas) and PTPN1 (Tyrosine-Protein Phosphatase Non-receptor type 1, also known as PTPB1, i.e. Protein-Tyrosine Phosphatase B1) were performed following incubation of HCT116 cells with 10 nM CBZ or 10 nM PEBCA-CBZ for 0.25 - 24 h (same samples as used for the lysosomal markers LAMP1, LAMP2a and cathepsin D described above). The results (Supplementary Figure 7C-D) reveal that both CSK and PTPN1 levels increased with time whether the cells were incubated with free CBZ or PEBCA-CBZ. The increase in these proteins might explain the time-dependent decrease in SRC, since the activity of these proteins will inactivate and mark SRC for degradation (Fan et al. 2015; Sievers et al. 2015). BCAR1, on the other hand, behaved differently in cells treated with free CBZ or PEBCA-CBZ as it was reduced similarly

to SRC for cells treated with PEBCA-CBZ, whereas it increased during the first 4 h of incubation with free CBZ before it decreased to approximately the same level as SRC after 24 h of incubation. The effect of CBZ on SRC was also seen in the other two cell lines (Supplementary Table 1), but the apparent corresponding rise in CSK levels was not detected. This could be due to the relatively low expression of CSK in these cell lines. Other SRC targets were reduced, such as BCAR1, particular for the breast cancer cell line.

Interestingly, as shown in Figure 9, the level of phosphorylation (the expected protein activity) of the SRC-kinase family targets VAMP7, RUNX3 and PLSCR1 were all reduced after CBZ-treatment, whereas the protein abundance was unaltered (WB for PLSCR1, data not shown). SRC kinase is a key regulator of several growth-signaling pathways (Espada and Martin-Perez 2017), and elevated levels of SRC kinase activity have been reported in a number of human cancers, including colon and breast cancer (Chen et al. 2014). SRC activation occurs in all stages of colon cancer metastasis and progression, and it has been presented as a biomarker for poor clinical prognosis of colon cancer (Wortmann et al. 2011). The SRC activity is regulated by tyrosine phosphorylations; positively at Y419 and negatively at Y527. The latter of these phosphorylations is mediated by CSK (thus the name C-terminal SRC kinase), which as described above is upregulated in the presence of CBZ, both in free and encapsulated form. Interestingly, this phosphorylated tyrosine can be dephosphorylated by PTPN1, found to be increased only under PEBCA-CBZ treatment. CSK is a non-receptor tyrosine-protein kinase that regulates cell growth, differentiation, migration and immune response, and phosphorylates tyrosine residues located in the C-terminal tails not only of SRC, but also of other SRC-family kinases such as LCK, HCK, FYN, LYN, CSK or YES1 (Indovina et al. 2017). CSK has been shown to suppress signaling by various surface receptors, including T- and B-cell receptors by phosphorylating and maintaining inactive several positive effectors such as FYN, SRC or LCK (Horejsi 2004; Machiyama et al. 2017).

The lack of observed effect of free CBZ and/or PACA-CBZ on YES1 (YES1 was included together with the analyses shown in Supplementary Figure 7C-D, but data for YES1 are not shown in the figure as no changes were observed), would indicate a more specific effect on the SRC pathway rather than a general effect on the SRC-family kinases.

The increased expression of the downstream SRC target CDCP1 (CUB domain-containing protein 1), would indicate a less favorable effect of SRC-reduction as discussed below. CDCP1 increased approximately 6x and 9x following incubation with free CBZ and PACA-CBZ, respectively. CDCP1 is a transmembrane tetraspanin protein involved in regulation of invasion and metastasis through tyrosine kinases (Orchard-Webb et al. 2014). It is a known substrate for SRC-family kinases which phosphorylates tyrosine residue Y743. It displays high expression in epithelial cells and is proposed as a prognostic unfavorable marker in several cancer types including lung (Ikeda et al. 2009) pancreatic cancer (Uekita et al. 2014), renal cell carcinoma (Awakura et al. 2008; Gao et al. 2013), ovarian cancer (Harrington et al. 2016), and hepatocellular carcinoma (Cao et al. 2016). A feedback loop via CD82/KAI1 from CDCP1 to SRC has been described where increased CDCP1 led to reduced SRC levels (Park et al. 2012).

It should be noted that the SRC-target protein BCAR1 was reduced to 63 and 58% of the control following incubation with free CBZ and PACA-CBZ, respectively (Western blot analyses showed a reduction to 70 % and 78%, respectively). BCAR1 is known as a docking protein which plays a central coordinating role for tyrosine kinase-based signaling related to cell adhesion (Hamasaki et al. 1996; Nojima et al. 1995; Zhang et al. 2017). It has been implicated in induction of cell migration and over-expression confers anti-estrogen resistance on breast cancer cells (Wallez et al. 2014). Furthermore, it has been shown to be regulated by PTPN1 (Liu et al. 2015), another SRC-regulated protein found to be enriched in our study. BCAR1 acts as a surface adaptor protein and bears similarities with focal adhesion proteins

such as FAK (Kumbrink et al. 2015). Reduction in the BCAR1 oncogene could be a very positive outcome of CBZ/PACA-CBZ-treatment for cancer progression.

Conclusion

Our data demonstrate that when cells are treated with CBZ encapsulated in PACA NPs, as compared to free CBZ, a number of pathways that are important for growth of cancer cells are targeted. Comparison of data obtained following proteomic and Western blot analyses of CBZ-loaded PEBCA nanoparticles and free CBZ revealed changes in the expression and phosphorylation of SRC-pathway proteins that may be related to the favorable therapeutic effect we recently reported of CBZ-loaded PEBCA compared to free CBZ on a patient derived xenograft model in mice.

Acknowledgements

We thank Anne Grethe Myrann for expert technical assistance with Western blotting analyses and Mara Stensland and Tuula Nyman at the Mass Spectrometry Core Facility at Oslo University Hospital for providing expertise access to equipment and performing MS analyses. Anne Rein Hatletveit at SINTEF is thanked for excellent technical assistance with production of nanoparticles.

Disclosure statement

No potential conflict of interest was reported by the authors.

Funding

This work was supported by The Research Council of Norway [NANO2021; project number 228200 (NANOCAN) and 274574 (nanoAUTOPHAGY), and the Norwegian Cancer Society.

ORCID

Anders Øverbye: http://orcid.org/0000-0002-2564-3729

Maria Lyngaas Torgersen: http://orcid.org/0000-0003-2616-7194

Tonje Sønstevold: http://orcid.org/0000-0003-2910-5618

Tore Geir Iversen: http://orcid.org/0000-0003-1148-6117

Ýrr Mørch: http://orcid.org/0000-0001-5182-7276

Tore Skotland: http://orcid.org/0000-0002-6524-612X

Kirsten Sandvig: http://orcid.org/ 0000-0002-4174-9072

FIGURE LEGENDS

Figure 1. Size distributions of the three types of PACAs studied both without drug and with encapsulated CBZ or DTX. PACAs without drug are shown with broken lines and CBZ-loaded PACAs are shown with solid lines: PBCAs (blue) PEBCAs (red) and POCAs (green). DTX-loaded PEBCAs are shown in rose.

Figure 2. *In vitro* toxicity measured using the MTT assay following incubation at 37 °C for 72 h with free CBZ, empty PACAs and CBZ-loaded PACAs with nine different cell lines. PACA-CBZ with 100 nM CBZ corresponds to 3.7-4.8 μg/ml PACA materials; equivalent amounts of empty PACA NPs were given for comparison. PACAs without drug are shown with broken lines and CBZ-loaded PACAs are shown with solid lines: PBCAs (blue) PEBCAs (red) and POCAs (green). Free CBZ is shown in black. The data shown for free CBZ, PEBCA-CBZ and empty PEBCA in MDA-MB-231, MDA-MB-468 and MCF-7 cells have recently been published (Fusser et al. 2019), but are included for comparison. The mean values ± SEM from three independent experiments are shown.

Figure 3. *In vitro* time dependent toxicity of free CBZ and CBZ-loaded PACAs in HT29 cells. The cells were incubated with the amount of substances indicated with the CBZ concentration on the x-axis for the time indicated within each part of the figure. The cells were then washed, and incubation continued at 37 °C for up to 72 h before toxicity was measured using the MTT assay. The data in the figure at the bottom labelled “72 h cont.” were obtained following continuous incubation with no washing. Free CBZ (black), PBCA-CBZ (blue), PEBCA-CBZ (red) and POCA-CBZ (green). The mean values ± SEM from three independent experiments are shown.

Figure 4. Comparison of the proteomes obtained after treatment of HCT116 cells with 3 and 10 nM CBZ, PBCA-PBZ, PEBCA-CBZ and POCA-CBZ. A. The number of proteins with significant ($p<0.01$) changes in protein levels after treatment with CBZ was in the range 200-300 proteins for each treatment. B. The amount of up-regulated versus down-regulated proteins for control cells versus CBZ-treated cells (ratio T:C). This ratio crosses the line with no changes (marked with an arrow) to the left of the mid-point demonstrating that there are more down-regulated than up-regulated proteins after treatment with CBZ.

Figure 5. Up-regulation and down-regulation of proteins in HCT116 cells treated for 24 h with CBZ versus untreated cells. Network changes for up-regulated proteins (A) and functional classification for up-regulated proteins (B). Network changes for down-regulated proteins (C) and functional classification for down-regulated proteins (D). Color marking of proteins in A: Nuclear proteins (blue), methylosome (green), phospholipase inhibitory function (red). Color marking of proteins in C: Focal adhesion proteins "dendrite" (blue), proteins involved in the ribonucleoprotein complex "establishment of ER localization" (red) translational proteins "ribonucleosomal" (green). Grey is used in both (A) and (C) to indicate proteins with classifications other than those specified in (B) and (D). The number of observed gene counts from the GO classification (i.e. number of proteins with changed levels) is shown in blue in (B) and (D); the numbers at the bottom show how many proteins are changed within each class. The red color in (B) and (D), i.e. that called "(-log) false discovery rate" (FDR), gives information about the probability of a correct classification which increases with a higher number at the bottom of each figure.

Figure 6. Up-regulation and down-regulation of proteins in HCT116 cells treated with high (10 nM) versus low (3 nM) concentrations of CBZ. Network changes for up-regulated proteins (A) and functional classification for up-regulated proteins (B). Network changes for down-regulated proteins (C) and functional classification for down-regulated proteins (D). Color marking of proteins in A: Ribonuclear proteins (green), cytoskeleton proteins (blue), and canonical glycolysis (red). Color marking of proteins in C: nuclear lumen (green), ribonucleoproteins (purple), establishment of ER localization (red), and rRNA binding (blue). Grey is used in both (A) and (C) to indicate proteins with classifications other than those specified in (B) and (D). The number of observed gene counts from the GO classification (i.e. number of proteins with changed levels) is shown in blue in (B) and (D); the numbers at the bottom show how many proteins are changed within each class. The red color in (B) and (D), i.e. that called "(-log) false discovery rate" (FDR), gives information about the probability of a correct classification which increases with a higher number at the bottom of each figure.

Figure 7. Up-regulation and down-regulation of proteins in HCT116 cells treated with CBZ-loaded PACAs versus cells treated with free CBZ. Network changes for up-regulated proteins (A) and functional classification for up-regulated proteins (B). Network changes for down-regulated proteins (C) and functional classification for down-regulated proteins (D). Color marking of proteins in A: Nuclear lumen (green), rho protein signal transduction (red), spliceosomal snRNP (blue), and XPC complex (orange). Color marking of proteins in C: RNA processing (blue), translational proteins (red), and stress fiber proteins (green). Grey is used in both (A) and (C) to indicate proteins with classifications other than those specified in (A) and (C). The number of observed gene counts from the GO classification (i.e. number of proteins with changed levels) is shown in blue in (B) and (D); the numbers at the bottom show how many proteins are changed within each class. The red color in (B) and (D), i.e. that called

“(-log) false discovery rate” (FDR), gives information about the probability of a correct classification which increases with a higher number at the bottom of each figure.

Figure 8. Comparison of protein groups detected above threshold for each of the cells lines HCT116, PC3 and MDA-MB-231 treated with PEBCA-CBZ and free CBZ (A). Transcriptome data published for these cells treated with CBZ (Shaul et al. 2016) are shown for comparison (B).

Figure 9. Proteins in the SRC pathway changed after CBZ treatment. Relationship between interactors of SRC affected by free CBZ or PACA-CBZ only. The symbols used are described in the figure. PTM: post translational modification.

References

Agafonov, D. E., J. Deckert, E. Wolf, P. Odenwalder, S. Bessonov, C. L. Will, H. Urlaub, and R. Luhrmann. 2011. "Semiquantitative proteomic analysis of the human spliceosome via a novel two-dimensional gel electrophoresis method." *Mol Cell Biol* 31 (13): 2667-2682. doi:10.1128/mcb.05266-11

Arpalahti, L., J. Hagstrom, H. Mustonen, M. Lundin, C. Haglund, and C. I. Holmberg. 2017. "UCHL5 expression associates with improved survival in lymph-node-positive rectal cancer." *Tumour Biol* 39 (7): 1010428317716078. doi:10.1177/1010428317716078

Ashburner, M., C. A. Ball, J. A. Blake, D. Botstein, H. Butler, J. M. Cherry, A. P. Davis, K. Dolinski, S. S. Dwight, J. T. Eppig, *et al.* 2000. "Gene ontology: tool for the unification of biology. The Gene Ontology Consortium." *Nat Genet* 25 (1): 25-29. doi:10.1038/75556

Aslund, A. K. O., E. Sulheim, S. Snipstad, E. von Haartman, H. Baghirov, N. Starr, M. Kvale Lovmo, S. Lelu, D. Scurr, C. L. Davies, *et al.* 2017. "Quantification and Qualitative Effects of Different PEGylations on Poly(butyl cyanoacrylate) Nanoparticles." *Mol Pharm* 14 (8): 2560-2569. doi:10.1021/acs.molpharmaceut.6b01085

Awakura, Y., E. Nakamura, T. Takahashi, H. Kotani, Y. Mikami, T. Kadowaki, A. Myoumoto, H. Akiyama, N. Ito, T. Kamoto, *et al.* 2008. "Microarray-based identification of CUB-domain containing protein 1 as a potential prognostic marker in conventional renal cell carcinoma." *J Cancer Res Clin Oncol* 134 (12): 1363-1369. doi:10.1007/s00432-008-0412-4

Baciarello, G., M. Gizzi, and K. Fizazi. 2018. "Advancing therapies in metastatic castration-resistant prostate cancer." *Expert Opin Pharmacother* 19 (16): 1797-1804. doi:10.1080/14656566.2018.1527312

Bjorkblom, B., A. Padzik, H. Mohammad, N. Westerlund, E. Komulainen, P. Hollos, L. Parviainen, A. C. Papageorgiou, K. Iljin, O. Kallioniemi, *et al.* 2012. "c-Jun N-terminal kinase phosphorylation of MARCKSL1 determines actin stability and migration in neurons and in cancer cells." *Mol Cell Biol* 32 (17): 3513-3526. doi:10.1128/MCB.00713-12

Buckland, A. G., and D. C. Wilton. 1998. "Inhibition of human cytosolic phospholipase A2 by human annexin V." *Biochem J* 329 (Pt 2) 369-372. doi:10.1042/bj3290369

Burridge, K., and C. Guilluy. 2016. "Focal adhesions, stress fibers and mechanical tension." *Exp Cell Res* 343 (1): 14-20. doi:10.1016/j.yexcr.2015.10.029

Cahn, F., and M. Lubin. 1978. "Inhibition of elongation steps of protein synthesis at reduced potassium concentrations in reticulocytes and reticulocyte lysate." *J Biol Chem* 253 (21): 7798-7803.

Cao, M., J. Gao, H. Zhou, J. Huang, A. You, Z. Guo, F. Fang, W. Zhang, T. Song, and T. Zhang. 2016. "HIF-2alpha regulates CDCP1 to promote PKCdelta-mediated migration in hepatocellular carcinoma." *Tumour Biol* 37 (2): 1651-1662. doi:10.1007/s13277-015-3527-7

Chadchankar, J., V. Korboukh, L. C. Conway, H. J. Wobst, C. A. Walker, P. Doig, S. J. Jacobsen, N. J. Brandon, S. J. Moss, and Q. Wang. 2019. "Inactive USP14 and inactive UCHL5 cause accumulation of distinct ubiquitinated proteins in mammalian cells." *PLoS One* 14 (11): e0225145. doi:10.1371/journal.pone.0225145

Chen, J., A. Elfiky, M. Han, C. Chen, and M. W. Saif. 2014. "The role of Src in colon cancer and its therapeutic implications." *Clin Colorectal Cancer* 13 (1): 5-13. doi:10.1016/j.clcc.2013.10.003

Clement, F. C., N. Kaczmarek, N. Mathieu, M. Tomas, A. Leitenstorfer, E. Ferrando-May, and H. Naegeli. 2011. "Dissection of the xeroderma pigmentosum group C protein

function by site-directed mutagenesis." *Antioxid Redox Signal* 14 (12): 2479-2490. doi:10.1089/ars.2010.3399
Cox, J., and M. Mann. 2008. "MaxQuant enables high peptide identification rates, individualized p.p.b.-range mass accuracies and proteome-wide protein quantification." *Nat Biotechnol* 26 (12): 1367-1372. doi:10.1038/nbt.1511
Duran, G. E., V. Derdau, D. Weitz, N. Philippe, J. Blankenstein, J. Atzrodt, D. Semiond, D. A. Gianolio, S. Mace, and B. I. Sikic. 2018. "Cabazitaxel is more active than first-generation taxanes in ABCB1(+) cell lines due to its reduced affinity for P-glycoprotein." *Cancer Chemother Pharmacol*. doi:10.1007/s00280-018-3572-1
Espada, J., and J. Martin-Perez. 2017. "An Update on Src Family of Nonreceptor Tyrosine Kinases Biology." *Int Rev Cell Mol Biol* 331 83-122. doi:10.1016/bs.ircmb.2016.09.009
Fan, G., S. Aleem, M. Yang, W. T. Miller, and N. K. Tonks. 2015. "Protein-tyrosine Phosphatase and Kinase Specificity in Regulation of SRC and Breast Tumor Kinase." *J Biol Chem* 290 (26): 15934-15947. doi:10.1074/jbc.M115.651703
Florian, M. C., K. J. Nattamai, K. Dorr, G. Marka, B. Uberle, V. Vas, C. Eckl, I. Andra, M. Schiemann, R. A. Oostendorp, *et al.* 2013. "A canonical to non-canonical Wnt signalling switch in haematopoietic stem-cell ageing." *Nature* 503 (7476): 392-396. doi:10.1038/nature12631
Friesen, W. J., A. Wyce, S. Paushkin, L. Abel, J. Rappsilber, M. Mann, and G. Dreyfuss. 2002. "A novel WD repeat protein component of the methylosome binds Sm proteins." *J Biol Chem* 277 (10): 8243-8247. doi:10.1074/jbc.M109984200
Fusser, M., A. Overbye, A. D. Pandya, Y. Morch, S. E. Borgos, W. Kildal, S. Snipstad, E. Sulheim, K. G. Fleten, H. A. Askautrud, *et al.* 2019. "Cabazitaxel-loaded Poly(2-ethylbutyl cyanoacrylate) nanoparticles improve treatment efficacy in a patient derived breast cancer xenograft." *J Control Release* 293 183-192. doi:10.1016/j.jconrel.2018.11.029
Gao, W., L. Chen, Z. Ma, Z. Du, Z. Zhao, Z. Hu, and Q. Li. 2013. "Isolation and phenotypic characterization of colorectal cancer stem cells with organ-specific metastatic potential." *Gastroenterology* 145 (3): 636-646.e635. doi:10.1053/j.gastro.2013.05.049
Gaudet, P., and C. Dessimoz. 2017. "Gene Ontology: Pitfalls, Biases, and Remedies." *Methods Mol Biol* 1446 189-205. doi:10.1007/978-1-4939-3743-1_14
Hamasaki, K., T. Mimura, N. Morino, H. Furuya, T. Nakamoto, S. Aizawa, C. Morimoto, Y. Yazaki, H. Hirai, and Y. Nojima. 1996. "Src kinase plays an essential role in integrin-mediated tyrosine phosphorylation of Crk-associated substrate p130Cas." *Biochem Biophys Res Commun* 222 (2): 338-343.
Harrington, B. S., Y. He, C. M. Davies, S. J. Wallace, M. N. Adams, E. A. Beaven, D. K. Roche, C. Kennedy, N. P. Chetty, A. J. Crandon, *et al.* 2016. "Cell line and patient-derived xenograft models reveal elevated CDCP1 as a target in high-grade serous ovarian cancer." *Br J Cancer* 114 (4): 417-426. doi:10.1038/bjc.2015.471
Hetz, C. 2012. "The unfolded protein response: controlling cell fate decisions under ER stress and beyond." *Nat Rev Mol Cell Biol* 13 (2): 89-102. doi:10.1038/nrm3270
Horejsi, V. 2004. "Transmembrane adaptor proteins in membrane microdomains: important regulators of immunoreceptor signaling." *Immunol Lett* 92 (1-2): 43-49. doi:10.1016/j.imlet.2003.10.013
Ikeda, J., T. Oda, M. Inoue, T. Uekita, R. Sakai, M. Okumura, K. Aozasa, and E. Morii. 2009. "Expression of CUB domain containing protein (CDCP1) is correlated with prognosis and survival of patients with adenocarcinoma of lung." *Cancer Sci* 100 (3): 429-433. doi:10.1111/j.1349-7006.2008.01066.x

Indovina, P., N. Casini, I. M. Forte, T. Garofano, D. Cesari, C. A. Iannuzzi, L. Del Porro, F. Pentimalli, L. Napoliello, S. Boffo, *et al.* 2017. "SRC Family Kinase Inhibition in Ewing Sarcoma Cells Induces p38 MAP Kinase-Mediated Cytotoxicity and Reduces Cell Migration." *J Cell Physiol* 232 (1): 129-135. doi:10.1002/jcp.25397

Iwai, S., A. Yonekawa, C. Harada, M. Hamada, W. Katagiri, M. Nakazawa, and Y. Yura. 2010. "Involvement of the Wnt-beta-catenin pathway in invasion and migration of oral squamous carcinoma cells." *Int J Oncol* 37 (5): 1095-1103.

Keich, U., K. Tamura, and W. S. Noble. 2018. "An averaging strategy to reduce variability in target-decoy estimates of false discovery rate." *J Proteome Res*. doi:10.1021/acs.jproteome.8b00802

Kim, S. M., P. H. Faix, and J. E. Schnitzer. 2017. "Overcoming key biological barriers to cancer drug delivery and efficacy." *J Control Release* 267 15-30. doi:10.1016/j.jconrel.2017.09.016

Kumbrink, J., S. Soni, B. Laumbacher, B. Loesch, and K. H. Kirsch. 2015. "Identification of Novel Crk-associated Substrate (p130Cas) Variants with Functionally Distinct Focal Adhesion Kinase Binding Activities." *J Biol Chem* 290 (19): 12247-12255. doi:10.1074/jbc.M115.649947

Lechel, A., and K. L. Rudolph. 2008. "Rho GTPase and Wnt signaling pathways in hepatocarcinogenesis." *Gastroenterology* 134 (3): 875-878. doi:10.1053/j.gastro.2008.01.055

Liu, H., Y. Wu, S. Zhu, W. Liang, Z. Wang, Y. Wang, T. Lv, Y. Yao, D. Yuan, and Y. Song. 2015. "PTP1B promotes cell proliferation and metastasis through activating src and ERK1/2 in non-small cell lung cancer." *Cancer Lett* 359 (2): 218-225. doi:10.1016/j.canlet.2015.01.020

Machioka, K., K. Izumi, Y. Kadono, H. Iwamoto, R. Naito, T. Makino, S. Kadomoto, A. Natsagdorj, E. T. Keller, J. Zhang, *et al.* 2018. "Establishment and characterization of two cabazitaxel-resistant prostate cancer cell lines." *Oncotarget* 9 (22): 16185-16196. doi:10.18632/oncotarget.24609

Machiyama, H., T. Yamaguchi, T. M. Watanabe, and H. Fujita. 2017. "A novel c-Src recruitment pathway from the cytosol to focal adhesions." *FEBS Lett* 591 (13): 1940-1946. doi:10.1002/1873-3468.12696

Mallick, S., and J. S. Choi. 2014. "Liposomes: versatile and biocompatible nanovesicles for efficient biomolecules delivery." *J Nanosci Nanotechnol* 14 (1): 755-765.

Matsumura, Y., and H. Maeda. 1986. "A new concept for macromolecular therapeutics in cancer chemotherapy: mechanism of tumoritropic accumulation of proteins and the antitumor agent smancs." *Cancer Res* 46 (12 Pt 1): 6387-6392.

Mita, A. C., R. Figlin, and M. M. Mita. 2012. "Cabazitaxel: more than a new taxane for metastatic castrate-resistant prostate cancer?" *Clin Cancer Res* 18 (24): 6574-6579. doi:10.1158/1078-0432.ccr-12-1584

Morch, Y., R. Hansen, S. Berg, A. K. Aslund, W. R. Glomm, S. Eggen, R. Schmid, H. Johnsen, S. Kubowicz, S. Snipstad, *et al.* 2015. "Nanoparticle-stabilized microbubbles for multimodal imaging and drug delivery." *Contrast Media Mol Imaging* 10 (5): 356-366. doi:10.1002/cmmi.1639

Nojima, Y., N. Morino, T. Mimura, K. Hamasaki, H. Furuya, R. Sakai, T. Sato, K. Tachibana, C. Morimoto, Y. Yazaki, *et al.* 1995. "Integrin-mediated cell adhesion promotes tyrosine phosphorylation of p130Cas, a Src homology 3-containing molecule having multiple Src homology 2-binding motifs." *J Biol Chem* 270 (25): 15398-15402.

Orchard-Webb, D. J., T. C. Lee, G. P. Cook, and G. E. Blair. 2014. "CUB domain containing protein 1 (CDCP1) modulates adhesion and motility in colon cancer cells." *BMC Cancer* 14 754. doi:10.1186/1471-2407-14-754

Pakos-Zebrucka, K., I. Koryga, K. Mnich, M. Ljujic, A. Samali, and A. M. Gorman. 2016. "The integrated stress response." *EMBO Rep* 17 (10): 1374-1395. doi:10.15252/embr.201642195

Paller, C. J., and E. S. Antonarakis. 2011. "Cabazitaxel: a novel second-line treatment for metastatic castration-resistant prostate cancer." *Drug Des Devel Ther* 5 117-124. doi:10.2147/dddt.s13029

Park, J. J., Y. B. Jin, Y. J. Lee, J. S. Lee, Y. S. Lee, Y. G. Ko, and M. Lee. 2012. "KAI1 suppresses HIF-1alpha and VEGF expression by blocking CDCP1-enhanced Src activation in prostate cancer." *BMC Cancer* 12 81. doi:10.1186/1471-2407-12-81

Peng, J., D. Schwartz, J. E. Elias, C. C. Thoreen, D. Cheng, G. Marsischky, J. Roelofs, D. Finley, and S. P. Gygi. 2003. "A proteomics approach to understanding protein ubiquitination." *Nat Biotechnol* 21 (8): 921-926. doi:10.1038/nbt849

Ruoslahti, E., S. N. Bhatia, and M. J. Sailor. 2010. "Targeting of drugs and nanoparticles to tumors." *J Cell Biol* 188 (6): 759-768. doi:10.1083/jcb.200910104

Santos, E., and P. Crespo. 2018. "The RAS-ERK pathway: A route for couples." *Sci Signal* 11 (554). doi:10.1126/scisignal.aav0917

Sapega, O., R. Mikyskova, J. Bieblova, B. Mrazkova, Z. Hodny, and M. Reinis. 2018. "Distinct phenotypes and 'bystander' effects of senescent tumour cells induced by docetaxel or immunomodulatory cytokines." *Int J Oncol* 53 (5): 1997-2009. doi:10.3892/ijo.2018.4553

Shaul, Y. D., B. Yuan, P. Thiru, A. Nutter-Upham, S. McCallum, C. Lanzkron, G. W. Bell, and D. M. Sabatini. 2016. "MERAV: a tool for comparing gene expression across human tissues and cell types." *Nucleic Acids Res* 44 (D1): D560-566. doi:10.1093/nar/gkv1337

Shi, Y., J. Conde, and H. S. Azevedo. 2017. "Empowering the Potential of Cell-Penetrating Peptides for Targeted Intracellular Delivery via Molecular Self-Assembly." *Adv Exp Med Biol* 1030 265-278. doi:10.1007/978-3-319-66095-0_12

Sievers, E., M. Trautmann, D. Kindler, S. Huss, I. Gruenewald, U. Dirksen, M. Renner, G. Mechtersheimer, F. Pedeutour, P. Aman, *et al.* 2015. "SRC inhibition represents a potential therapeutic strategy in liposarcoma." *Int J Cancer* 137 (11): 2578-2588. doi:10.1002/ijc.29645

Sindhwani, S., A. M. Syed, J. Ngai, B. R. Kingston, L. Maiorino, J. Rothschild, P. MacMillan, Y. Zhang, N. U. Rajesh, T. Hoang, *et al.* 2020. "The entry of nanoparticles into solid tumours." *Nat Mater* 19 (5): 566-575. doi:10.1038/s41563-019-0566-2

Skotland, T., and K. Sandvig. 2021. "Transport of nanoparticles across the endothelial cell layer." *Nano Today* 36 101029.

Smiyun, G., O. Azarenko, H. Miller, A. Rifkind, N. E. LaPointe, L. Wilson, and M. A. Jordan. 2017. "betaIII-tubulin enhances efficacy of cabazitaxel as compared with docetaxel." *Cancer Chemother Pharmacol* 80 (1): 151-164. doi:10.1007/s00280-017-3345-2

Stockert, J. C., R. W. Horobin, L. L. Colombo, and A. Blazquez-Castro. 2018. "Tetrazolium salts and formazan products in Cell Biology: Viability assessment, fluorescence imaging, and labeling perspectives." *Acta Histochem* 120 (3): 159-167. doi:10.1016/j.acthis.2018.02.005

Sulheim, E., H. Baghirov, E. von Haartman, A. Boe, A. K. Aslund, Y. Morch, and L. Davies Cde. 2016. "Cellular uptake and intracellular degradation of poly(alkyl cyanoacrylate) nanoparticles." *J Nanobiotechnology* 14 1. doi:10.1186/s12951-015-0156-7

Sulheim, E., T. G. Iversen, V. To Nakstad, G. Klinkenberg, H. Sletta, R. Schmid, A. R. Hatletveit, A. M. Wagbo, A. Sundan, T. Skotland, *et al.* 2017. "Cytotoxicity of

Poly(Alkyl Cyanoacrylate) Nanoparticles." *Int J Mol Sci* 18 (11). doi:10.3390/ijms18112454

Szwed, M., T. Sonstevold, A. Overbye, N. Engedal, B. Grallert, Y. Morch, E. Sulheim, T. G. Iversen, T. Skotland, K. Sandvig, *et al.* 2019. "Small variations in nanoparticle structure dictate differential cellular stress responses and mode of cell death." *Nanotoxicology* 1-22. doi:10.1080/17435390.2019.1576238

Szwed, M., M. L. Torgersen, R. V. Kumari, S. K. Yadava, S. Pust, T. G. Iversen, T. Skotland, J. Giri, and K. Sandvig. 2020. "Biological response and cytotoxicity induced by lipid nanocapsules." *J Nanobiotechnology* 18 (1): 5. doi:10.1186/s12951-019-0567-y

Sønstevold, T., N. Engedal, Ý. Mørch, T. G. Iversen, T. Skotland, K. Sandvig, and M. L. Torgersen. 2020. "Structural Variants of poly(alkylcyanoacrylate) Nanoparticles Differentially Affect LC3 and Autophagic Cargo Degradation." *Journal of Biomedical Nanotechnology* 16 (4): 432-445. doi:10.1166/jbn.2020.2906

Taurin, S., H. Nehoff, and K. Greish. 2012. "Anticancer nanomedicine and tumor vascular permeability; Where is the missing link?" *J Control Release* 164 (3): 265-275. doi:10.1016/j.jconrel.2012.07.013

Tcatchoff, L., S. Andersson, A. Utskarpen, T. I. Klokk, S. S. Skanland, S. Pust, V. Gerke, and K. Sandvig. 2012. "Annexin A1 and A2: roles in retrograde trafficking of Shiga toxin." *PLoS One* 7 (7): e40429. doi:10.1371/journal.pone.0040429

Torchilin, V. P. 2014. "Multifunctional, stimuli-sensitive nanoparticulate systems for drug delivery." *Nat Rev Drug Discov* 13 (11): 813-827. doi:10.1038/nrd4333

Uekita, T., S. Fujii, Y. Miyazawa, R. Iwakawa, M. Narisawa-Saito, K. Nakashima, K. Tsuta, H. Tsuda, T. Kiyono, J. Yokota, *et al.* 2014. "Oncogenic Ras/ERK signaling activates CDCP1 to promote tumor invasion and metastasis." *Mol Cancer Res* 12 (10): 1449-1459. doi:10.1158/1541-7786.mcr-13-0587

Vauthier, C., C. Dubernet, C. Chauvierre, I. Brigger, and P. Couvreur. 2003. "Drug delivery to resistant tumors: the potential of poly(alkyl cyanoacrylate) nanoparticles." *J Control Release* 93 (2): 151-160.

Vrignaud, P., D. Semiond, P. Lejeune, H. Bouchard, L. Calvet, C. Combeau, J. F. Riou, A. Commercon, F. Lavelle, and M. C. Bissery. 2013. "Preclinical antitumor activity of cabazitaxel, a semisynthetic taxane active in taxane-resistant tumors." *Clin Cancer Res* 19 (11): 2973-2983. doi:10.1158/1078-0432.ccr-12-3146

Wallez, Y., S. J. Riedl, and E. B. Pasquale. 2014. "Association of the breast cancer antiestrogen resistance protein 1 (BCAR1) and BCAR3 scaffolding proteins in cell signaling and antiestrogen resistance." *J Biol Chem* 289 (15): 10431-10444. doi:10.1074/jbc.M113.541839

Will, C. L., and R. Luhrmann. 2011. "Spliceosome structure and function." *Cold Spring Harb Perspect Biol* 3 (7). doi:10.1101/cshperspect.a003707

Wortmann, A., Y. He, M. E. Christensen, M. Linn, J. W. Lumley, P. M. Pollock, N. J. Waterhouse, and J. D. Hooper. 2011. "Cellular settings mediating Src Substrate switching between focal adhesion kinase tyrosine 861 and CUB-domain-containing protein 1 (CDCP1) tyrosine 734." *J Biol Chem* 286 (49): 42303-42315. doi:10.1074/jbc.M111.227462

Zhang, C., D. J. Miller, C. D. Guibao, D. M. Donato, S. K. Hanks, and J. J. Zheng. 2017. "Structural and functional insights into the interaction between the Cas family scaffolding protein p130Cas and the focal adhesion-associated protein paxillin." *J Biol Chem* 292 (44): 18281-18289. doi:10.1074/jbc.M117.807271

Figure 1.

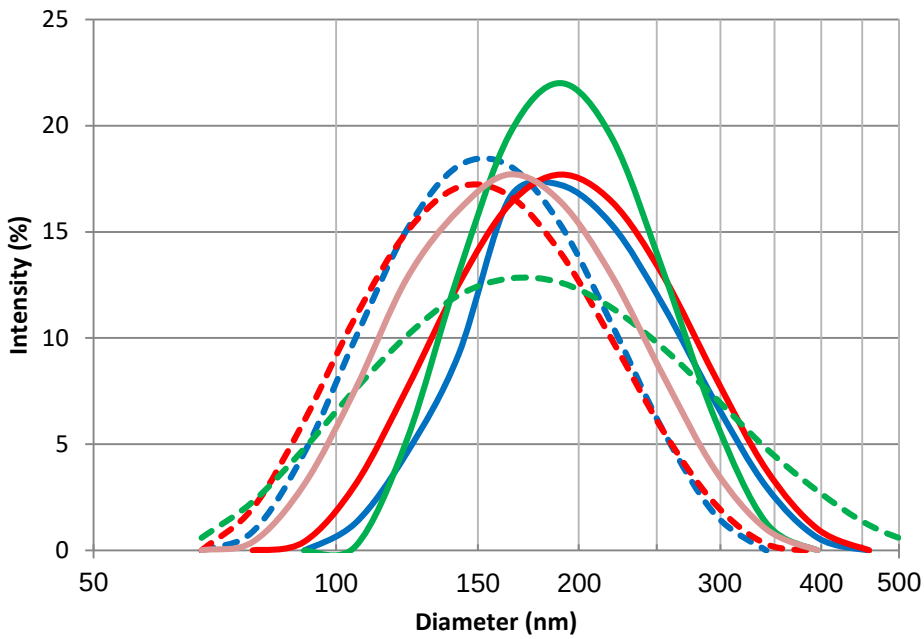

Figure 2.

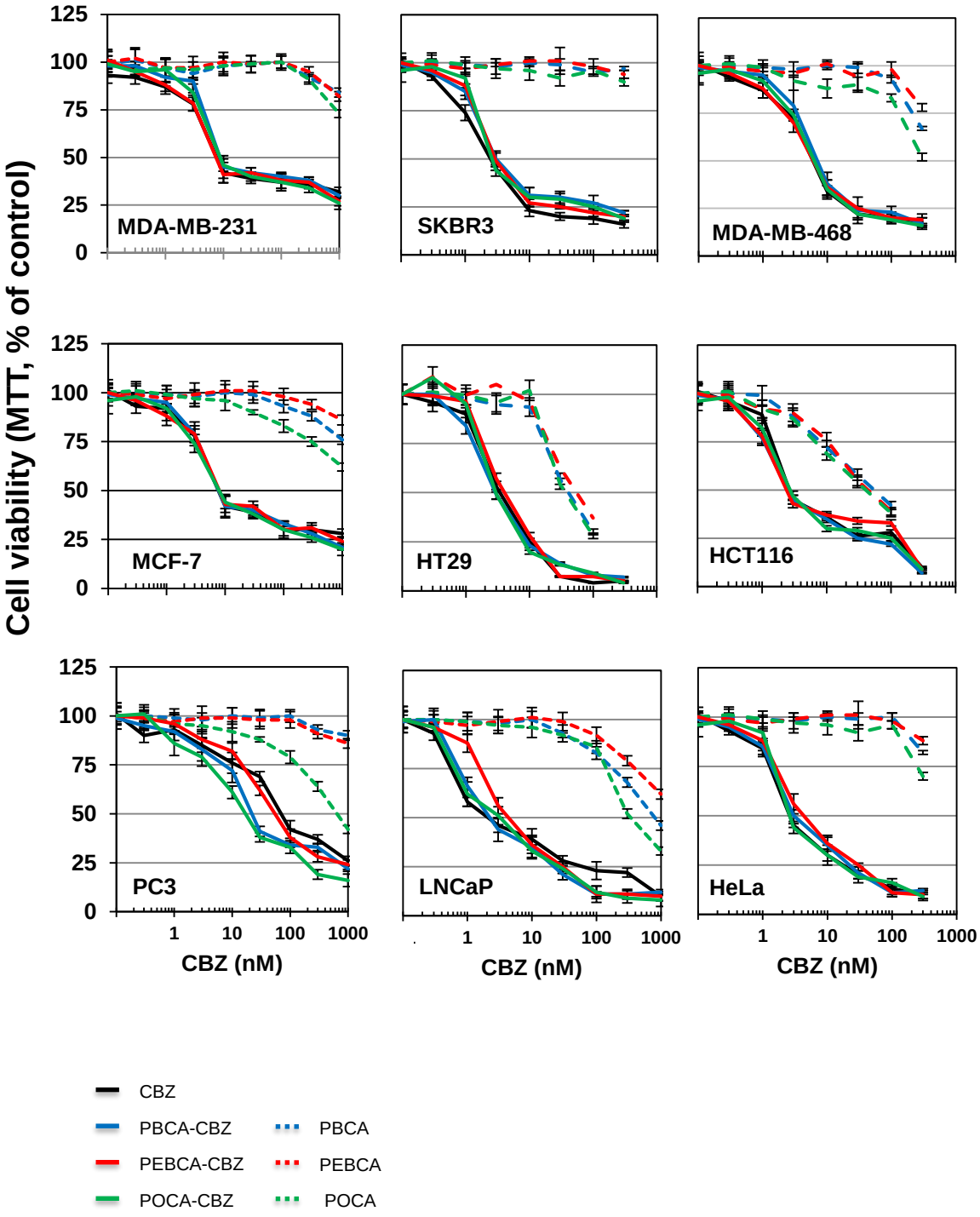
Cell viability (MTT, % of control)
125
100
75
50
25
0
MDA-MB-231
SKBR3
MDA-MB-468
MCF-7
HT29
HCT116
PC3
LNCaP
HeLa
1
10
100
1000
CBZ (nM)
CBZ
PBCA-CBZ
PEBCA-CBZ
POCA-CBZ
PBCA
PEBCA
POCA

Figure 3.

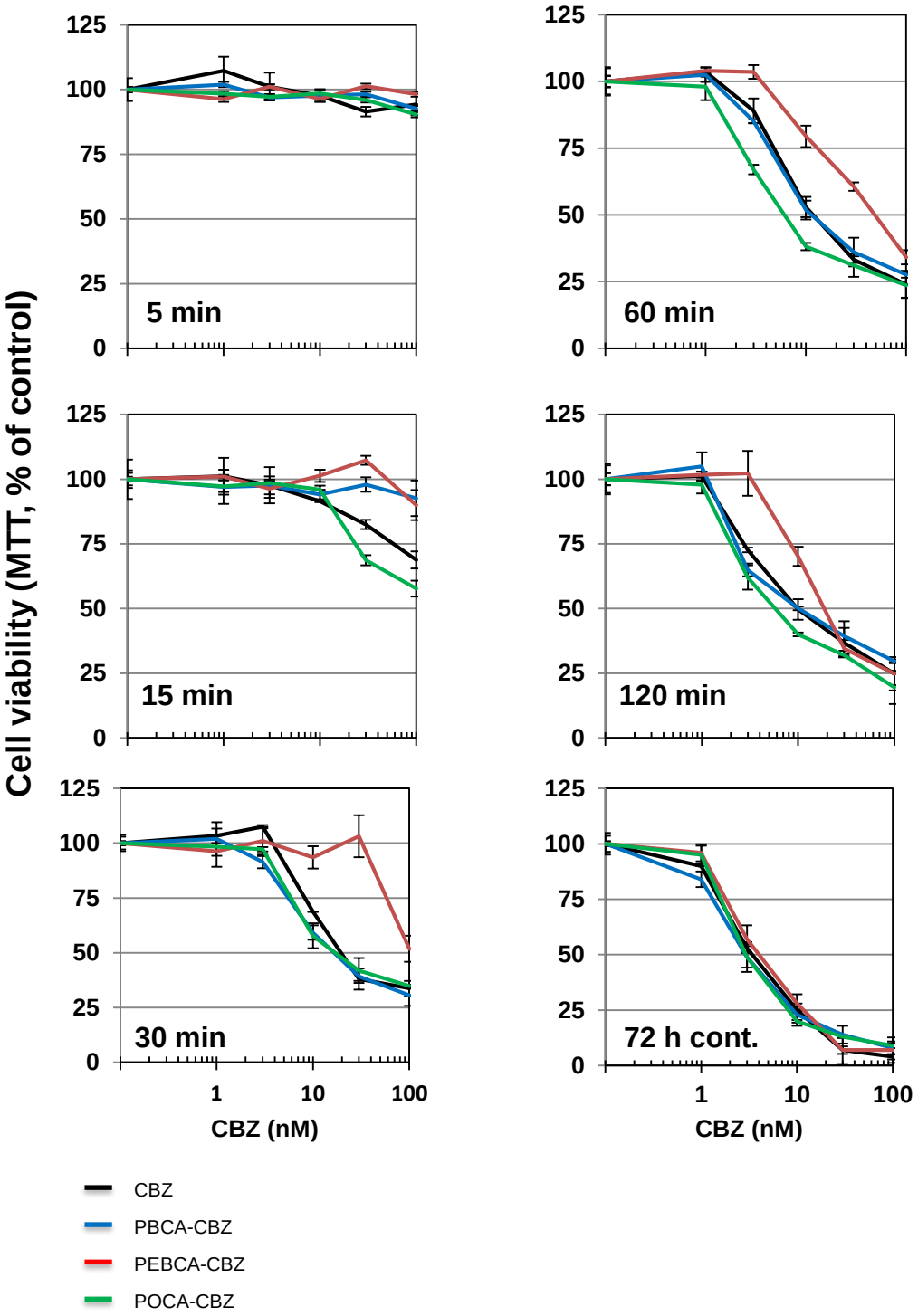
Cell viability (MTT, % of control)
125
100
75
50
25
0
5 min
60 min
15 min
120 min
30 min
72 h cont.
1
10
100
CBZ (nM)
CBZ
PBCA-CBZ
PEBCA-CBZ
POCA-CBZ

Figure 4.

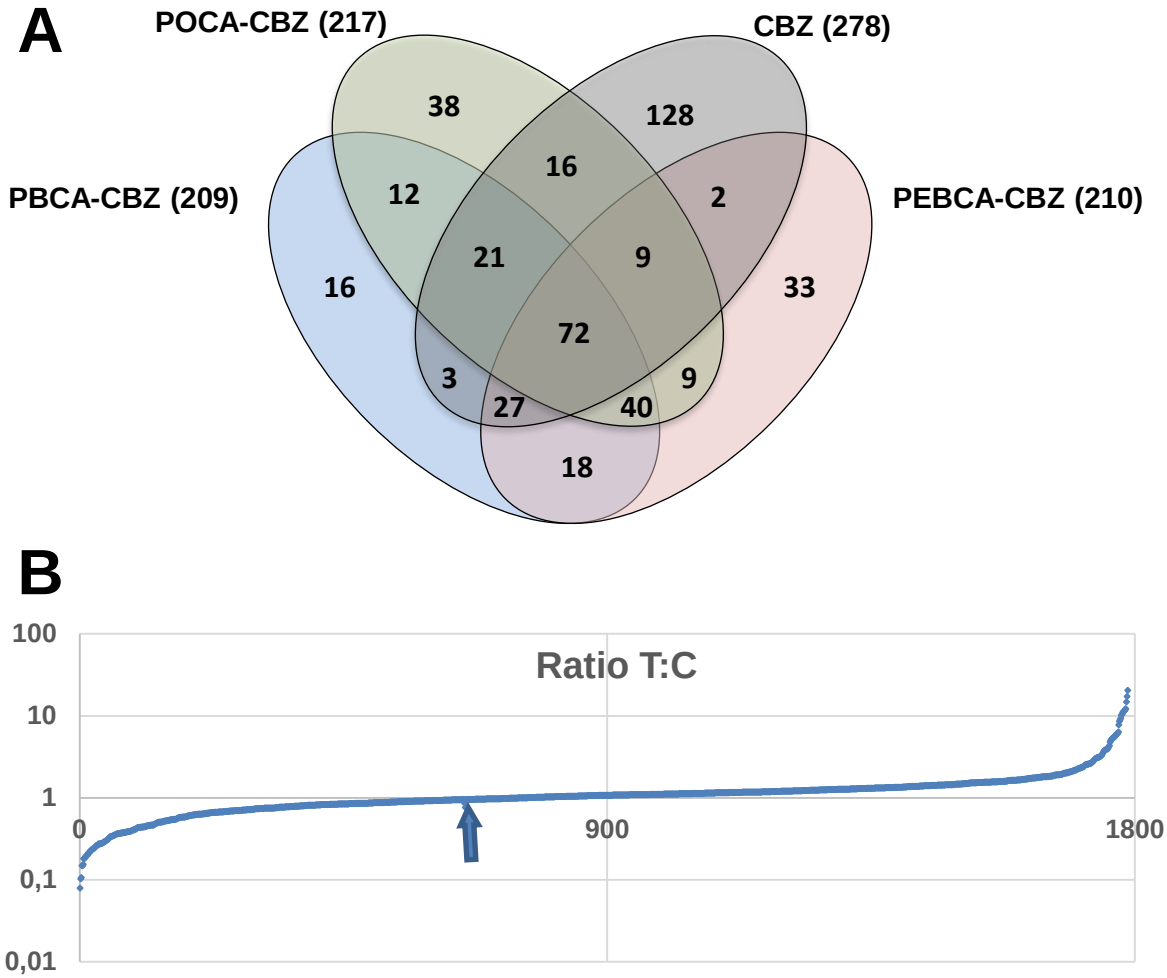
A
POCA-CBZ (217)
CBZ (278)
PBCA-CBZ (209)
PEBCA-CBZ (210)
38
128
16
12
2
21
9
16
33
72
3
9
27
40
18
B
Ratio T:C
100
10
1
0,1
0,01
0
900
1800

Figure 5.

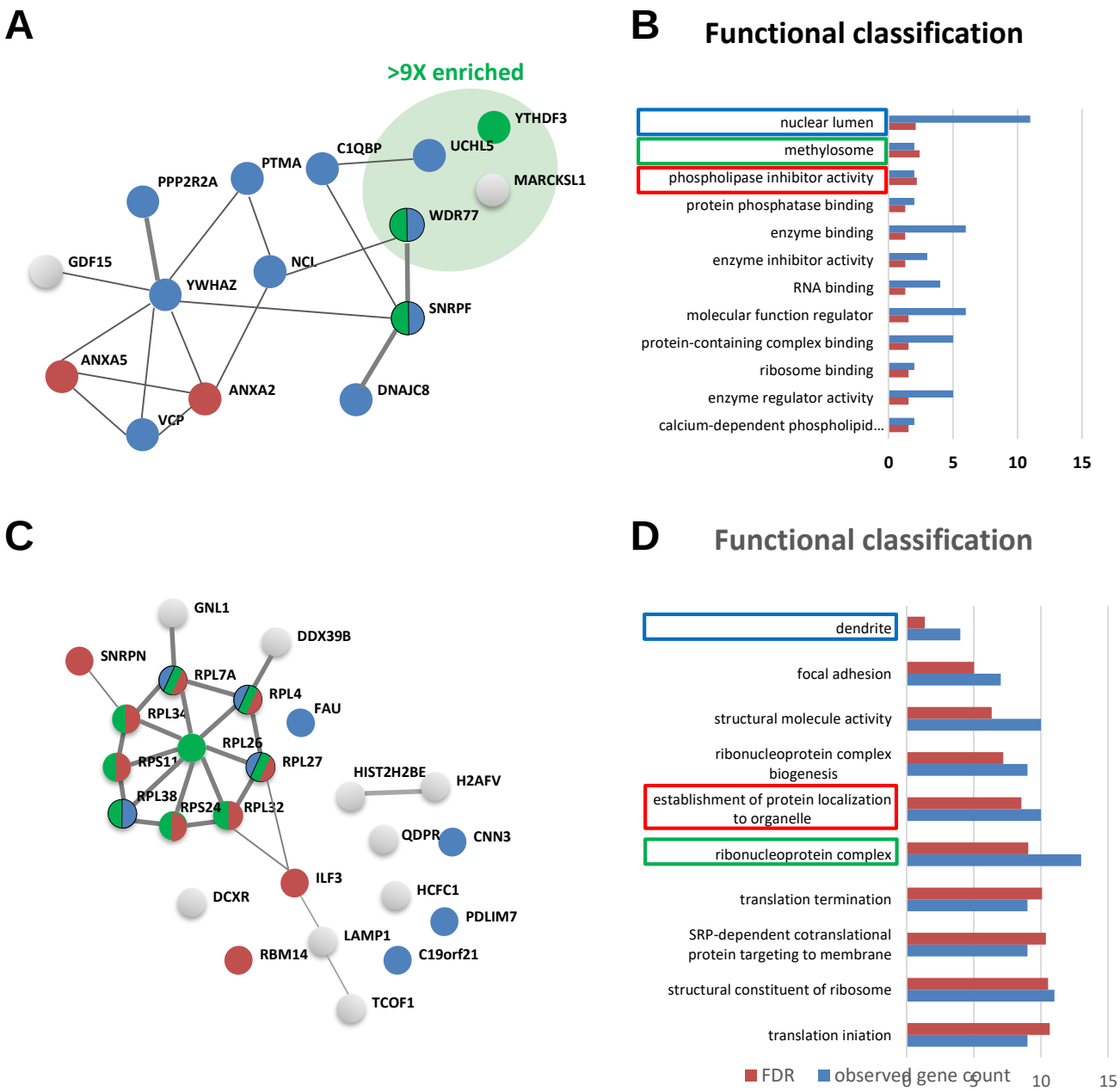
A
>9X enriched
YTHDF3
UCHL5
C1QBP
PTMA
PPP2R2A
MARCKSL1
WDR77
GDF15
NCL
YWHAZ
SNRPF
ANXA5
ANXA2
DNAJC8
VCP
B
Functional classification
nuclear lumen
methylosome
phospholipase inhibitor activity
protein phosphatase binding
enzyme binding
enzyme inhibitor activity
RNA binding
molecular function regulator
protein-containing complex binding
ribosome binding
enzyme regulator activity
calcium-dependent phospholipid...
0
5
10
15
C
GNL1
DDX39B
SNRPN
RPL7A
RPL4
FAU
RPL34
RPL26
RPS11
RPL27
HIST2H2BE
H2AFV
RPL38
RPS24
RPL32
QDPR
CNN3
ILF3
DCXR
HCFC1
PDLIM7
LAMP1
RBM14
C19orf21
TCOF1
D
Functional classification
dendrite
focal adhesion
structural molecule activity
ribonucleoprotein complex biogenesis
establishment of protein localization to organelle
ribonucleoprotein complex
translation termination
SRP-dependent cotranslational protein targeting to membrane
structural constituent of ribosome
translation iniation
FDR
observed gene count
0
5
10
15

Figure 6.

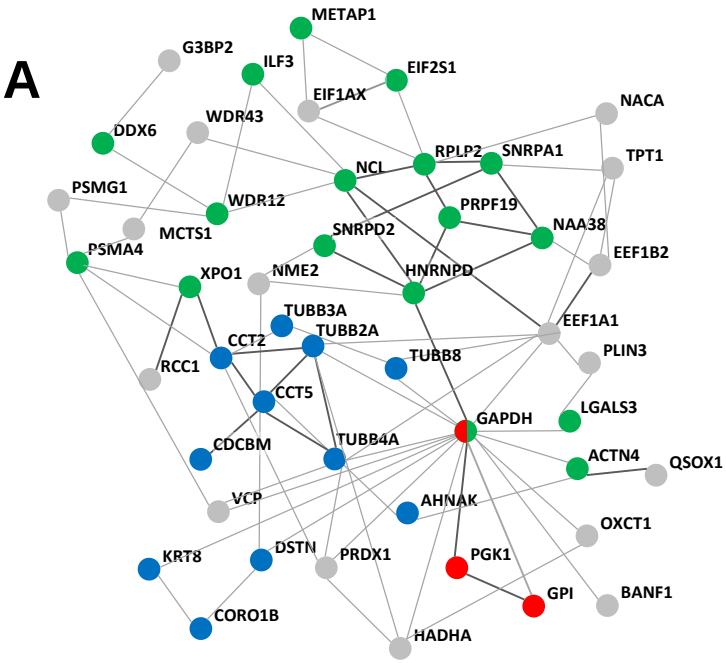
A
METAP1
G3BP2
ILF3
EIF2S1
EIF1AX
NACA
DDX6
WDR43
RPLP2
SNRPA1
TPT1
NCL
PSMG1
WDR12
PRPF19
MCTS1
SNRPD2
NAA38
PSMA4
EEF1B2
XPO1
NME2
HNRNPD
TUBB3A
EEF1A1
CCT2
TUBB2A
PLIN3
RCC1
TUBB8
CCT5
LGALS3
GAPDH
CDCBM
TUBB4A
ACTN4
QSOX1
VCP
AHNAK
OXCT1
KRT8
DSTN
PRDX1
PGK1
GPI
BANF1
CORO1B
HADHA

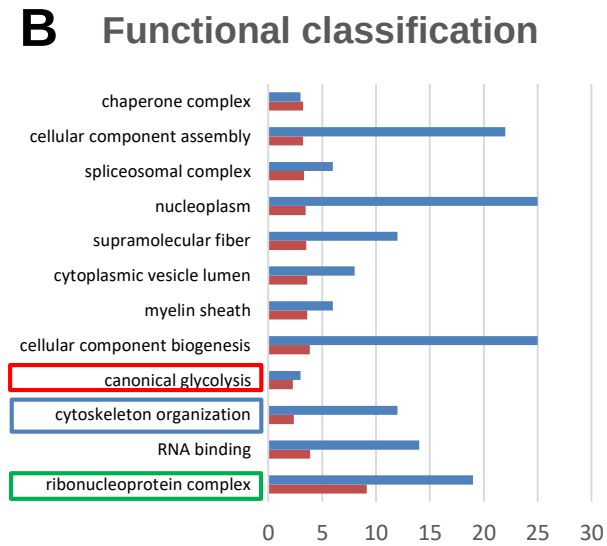
B
Functional classification
chaperone complex
cellular component assembly
spliceosomal complex
nucleoplasm
supramolecular fiber
cytoplasmic vesicle lumen
myelin sheath
cellular component biogenesis
canonical glycolysis
cytoskeleton organization
RNA binding
ribonucleoprotein complex
0
5
10
15
20
25
30

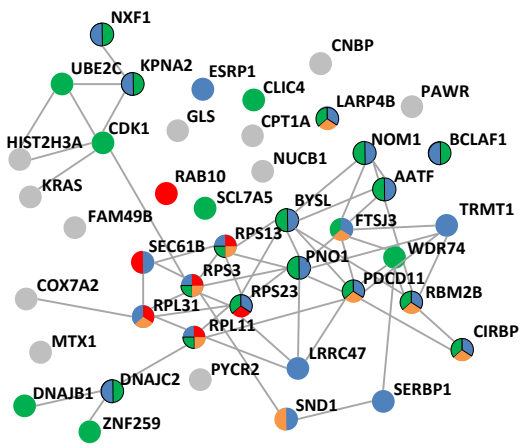
C
NXF1
CNBP
UBE2C
KPNA2
ESRP1
CLIC4
LARP4B
PAWR
GLS
CPT1A
HIST2H3A
CDK1
NOM1
BCLAF1
NUCB1
RAB10
AATF
KRAS
SCL7A5
BYSL
TRMT1
FAM49B
FTSJ3
RPS13
SEC61B
WDR74
PNO1
RPS3
PDCD11
COX7A2
RPS23
RBM2B
RPL31
RPL11
CIRBP
MTX1
LRRC47
PYCR2
DNAJC2
SERBP1
DNAJB1
SND1
ZNF259

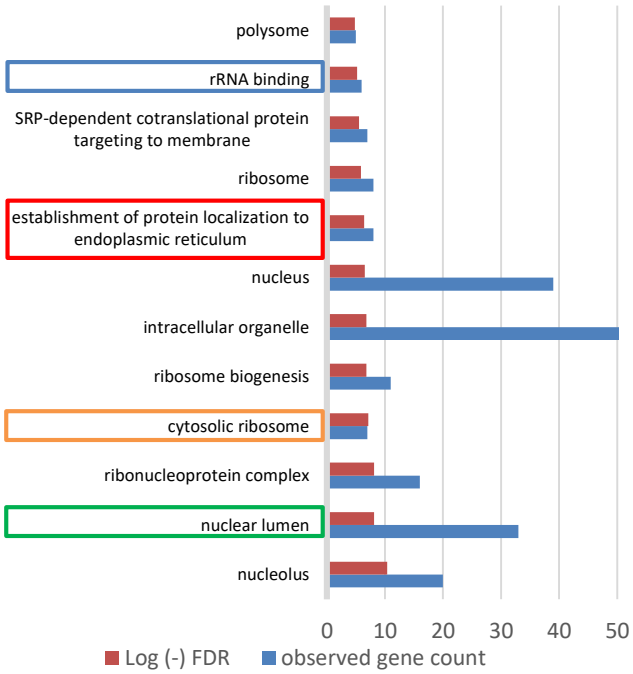
D
Functional classification
polysome
rRNA binding
SRP-dependent cotranslational protein targeting to membrane
ribosome
establishment of protein localization to endoplasmic reticulum
nucleus
intracellular organelle
ribosome biogenesis
cytosolic ribosome
ribonucleoprotein complex
nuclear lumen
nucleolus
0
10
20
30
40
50
Log (-) FDR
observed gene count

Figure 7.

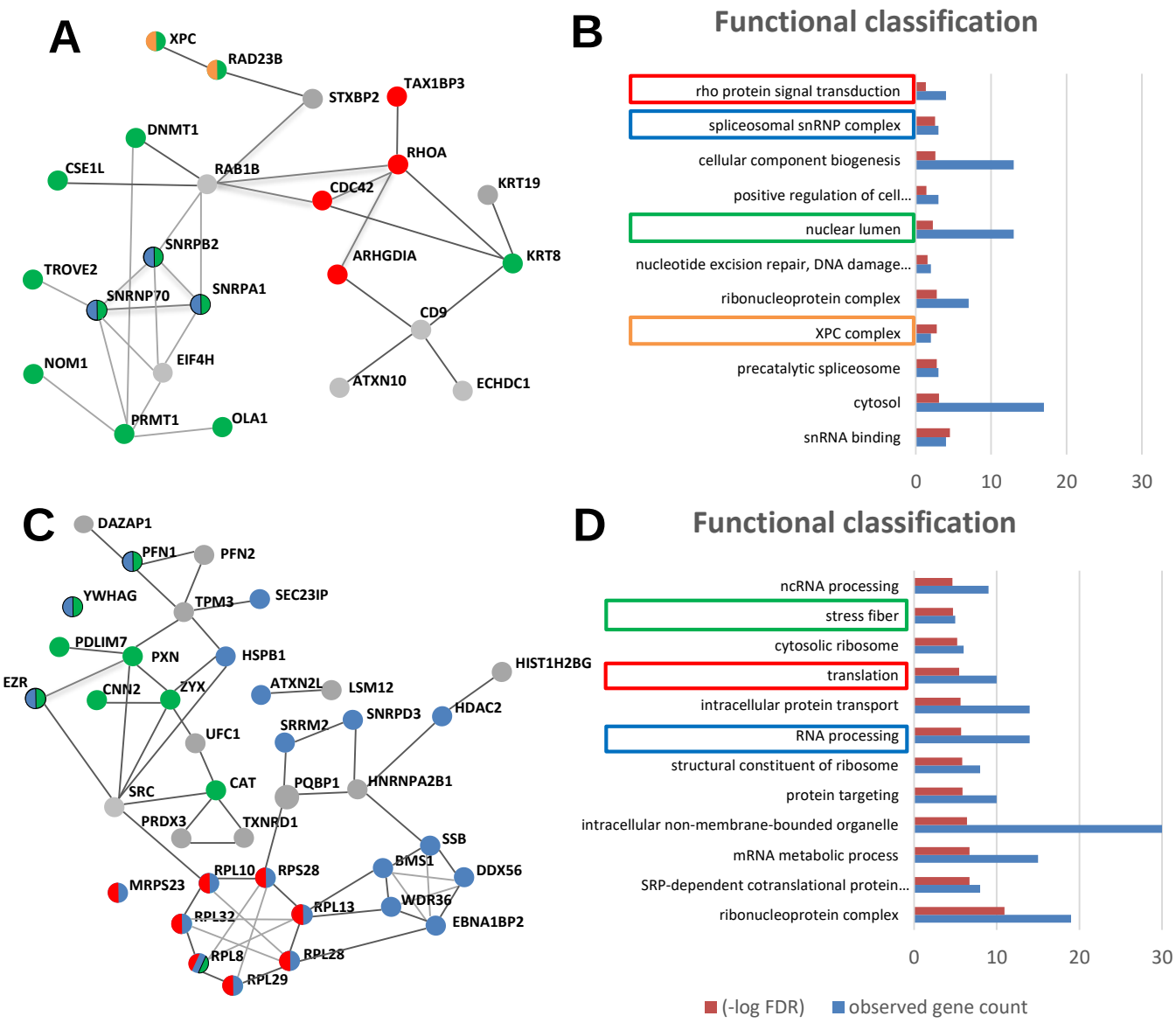
A
XPC
RAD23B
STXBP2
TAX1BP3
DNMT1
RHOA
CSE1L
RAB1B
CDC42
KRT19
SNRPB2
ARHGDIA
KRT8
TROVE2
SNRNP70
SNRPA1
CD9
NOM1
EIF4H
ATXN10
ECHDC1
PRMT1
OLA1
B
Functional classification
rho protein signal transduction
spliceosomal snRNP complex
cellular component biogenesis
positive regulation of cell...
nuclear lumen
nucleotide excision repair, DNA damage...
ribonucleoprotein complex
XPC complex
precatalytic spliceosome
cytosol
snRNA binding
0
10
20
30
C
DAZAP1
PFN1
PFN2
YWHAG
TPM3
SEC23IP
PDLIM7
PXN
HSPB1
HIST1H2BG
EZR
CNN2
ZYX
ATXN2L
LSM12
SNRPD3
HDAC2
SRRM2
UFC1
SRC
CAT
PQBP1
HNRNPA2B1
PRDX3
TXNRD1
SSB
BMS1
DDX56
MRPS23
RPL10
RPS28
WDR36
RPL13
RPL32
EBNA1BP2
RPL8
RPL28
RPL29
D
Functional classification
ncRNA processing
stress fiber
cytosolic ribosome
translation
intracellular protein transport
RNA processing
structural constituent of ribosome
protein targeting
intracellular non-membrane-bounded organelle
mRNA metabolic process
SRP-dependent cotranslational protein...
ribonucleoprotein complex
0
10
20
30
(-log FDR)
observed gene count

Figure 8.

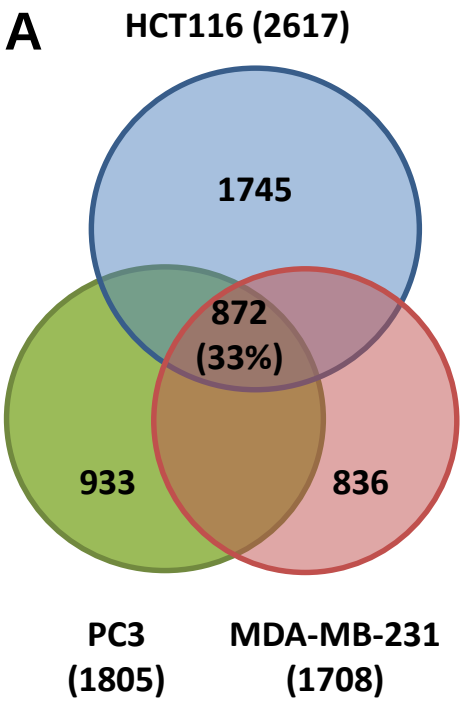

Proteins detected (medium threshold)

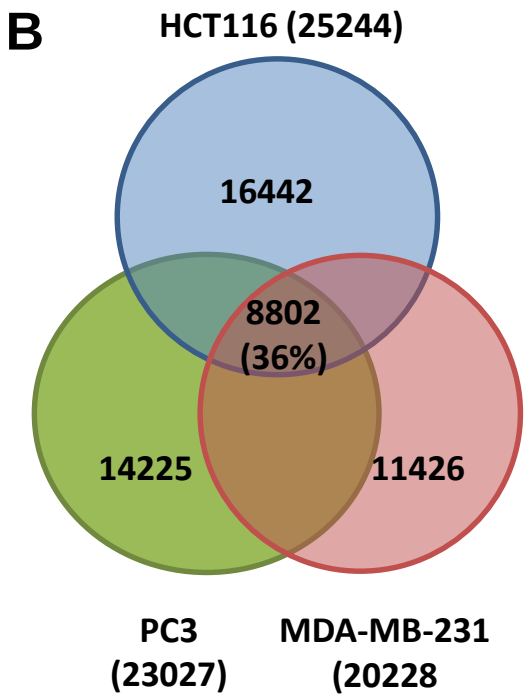

Genes expressed (medium threshold)

Figure 9.

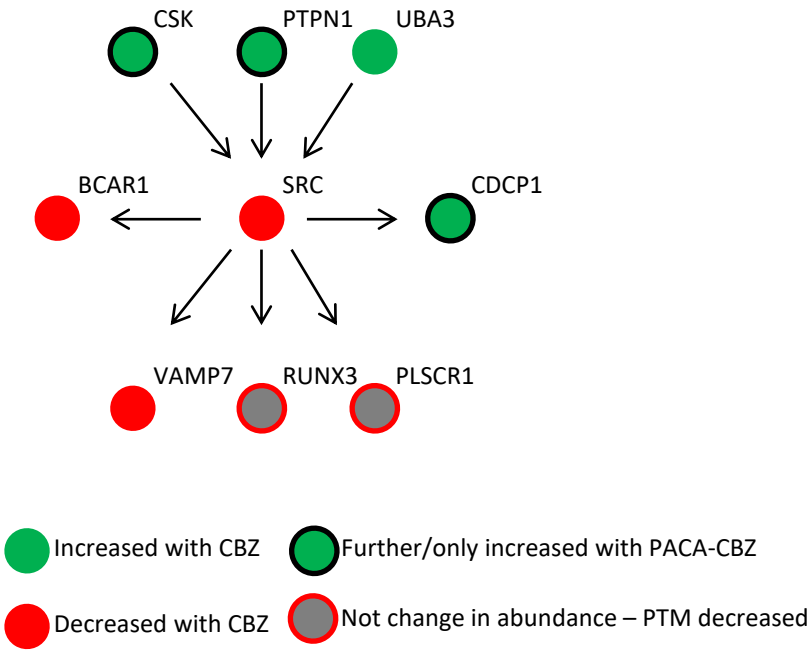
CSK
PTPN1
UBA3
BCAR1
SRC
CDCP1
VAMP7
RUNX3
PLSCR1
Increased with CBZ
Further/only increased with PACA-CBZ
Decreased with CBZ
Not change in abundance – PTM decreased

Table 1. Characterization of empty and drug-loaded PACA NPs used in the present study.

PACA	Diameter z-avg. (nm)	PDI	Zeta potential (mV)	NP dry weight (mg/ml)	CBZ (% of NP dry weight)
PBCA	129	0.11	-3.2	27	-
PBCA-CBZ	209	0.10	-3.0	6	4.4
PEBCA	153	0.13	-2.4	37	-
PEBCA-CBZ	182	0.08	-1.0	7	4.1
PEBCA-DTX	149	0.24	-1.3	5	1.2
POCA	147	0.12	-5.2	16	-
POCA-CBZ	181	0.18	-0.5	19	1.0

Table 2. Overview of the different comparison analyses performed using the proteomic analyses. Colors indicate different PACA-package material (blue PBCA, red PEBCA, green POCA), black dots indicate drug presence (CBZ), the number of the dots depicts concentration. An alternative way to illustrate Scenario 1-3 is shown in Supplementary Figure 6.

Scenario	Comparison of proteomic data	Illustration
1	Comparing effect obtained by any CBZ treatment with control or empty PEBCA	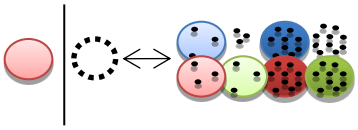
2	Comparing effect obtained using 3 nM versus 10 nM CBZ	
3	Comparing free CBZ with CBZ-loaded PACAs	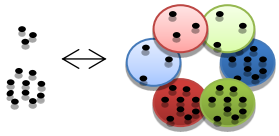
4	Comparing effect obtained with the different PACAs	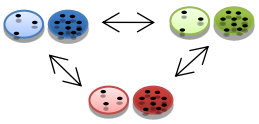
5	Comparison of effects obtained with the three cell lines	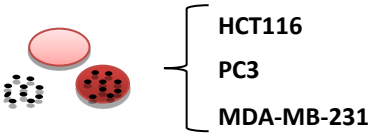

Supplementary file

Cabazitaxel-loaded poly(alkyl cyanoacrylate) nanoparticles: Toxicity and changes in the proteome of breast, colon and prostate cancer cells

Anders Øverbye[a], Maria Lyngaas Torgersen[a], Tonje Sønstevold[a,b], Tore Geir Iversen[a], Ýrr Mørch[c], Tore Skotland[a], and Kirsten Sandvig[a,b,*]

[a] Department of Molecular Cell Biology, Institute for Cancer Research, Oslo University Hospital, The Norwegian Radium Hospital, Oslo, Norway

[b] Department of Biosciences, University of Oslo, Oslo, Norway

[c] Department of Biotechnology and Nanomedicine, SINTEF AS, Trondheim, Norway

* Communicating author: ksandvig@radium.uio.no

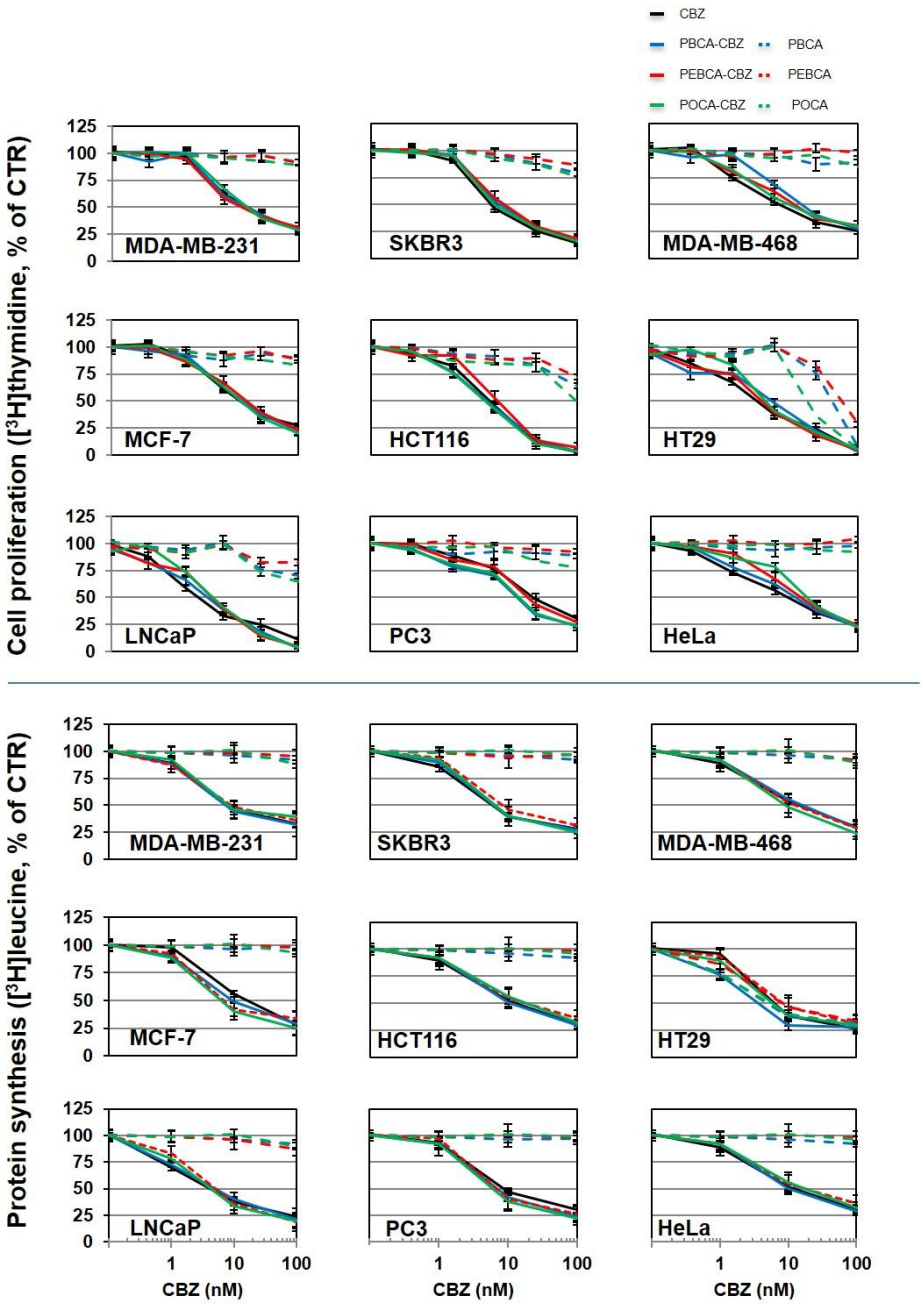

Supplementary Figure 1. Effect of PACAs on cell proliferation and protein synthesis. The effect on cell proliferation was measured by incorporation of [^{3}H]thymidine following 24 h incubation of the nine cell lines with the different substances (top nine panels). The effect on protein synthesis was measured by incorporation of [^{3}H]leucine following 24 h incubation of the nine cell lines with the different substances (bottom nine panels). PACAs without drug are shown with broken lines and drug-loaded PACAs are shown with solid lines: PBCAs (blue) PEBCAs (red) and POCAs (green). Free CBZ is shown in black. PACAs without drug were added at equivalent amounts as the drug-loaded PACAs. The mean values ± SEM from three independent experiments are shown.

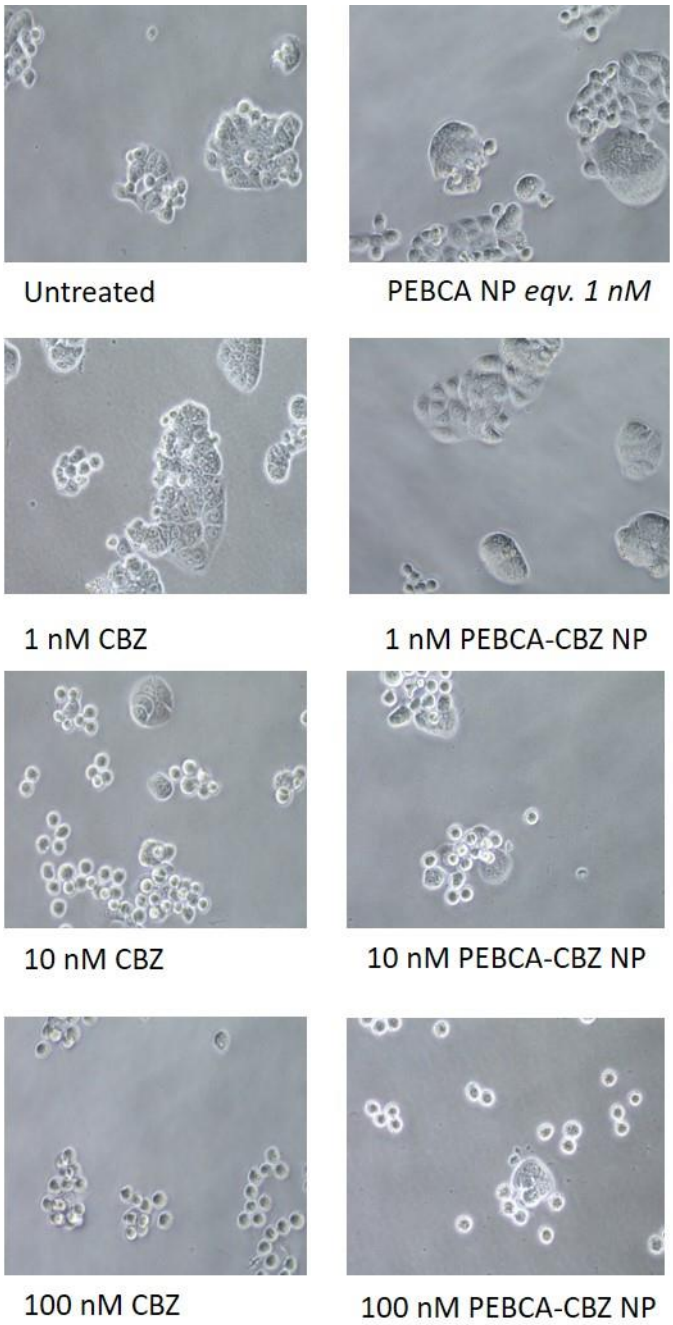

Supplementary Figure 2. Morphology of HCT116 cells following incubation with PEBCA, PEBCA-CBZ or free CBZ as well as untreated cells. HCT116 cells were seeded in 24-well plates (50,000 cells per well) and incubated for 24 h at the conditions indicated below each of the micrographs (concentrations given are for CBZ), which were taken with a 20x objective.

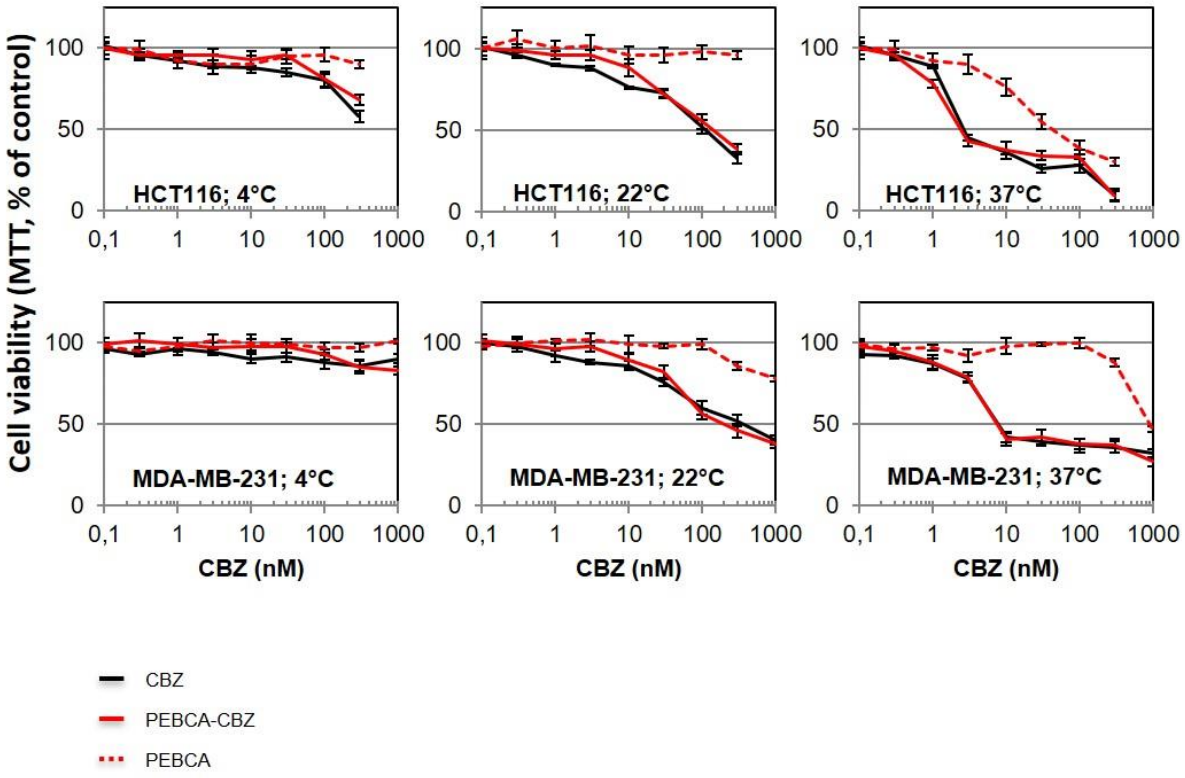

Supplementary Figure 3. *In vitro* toxicity measured following incubation of cells with substances for 2 h at 4, 22 or 37 °C followed by washing of the cells and further incubation of samples at 37 °C for 70 h; then the cells were analyzed using the MTT assay. Data obtained with the HCT116 cells are shown in the upper row and data obtained with the MDA-MB-231 cells are shown in the lower row. Symbols used: Free CBZ (black), PEBCA-CBZ (solid red) and empty PEBCA (broken red). The mean values ± SEM from three independent experiments are shown.

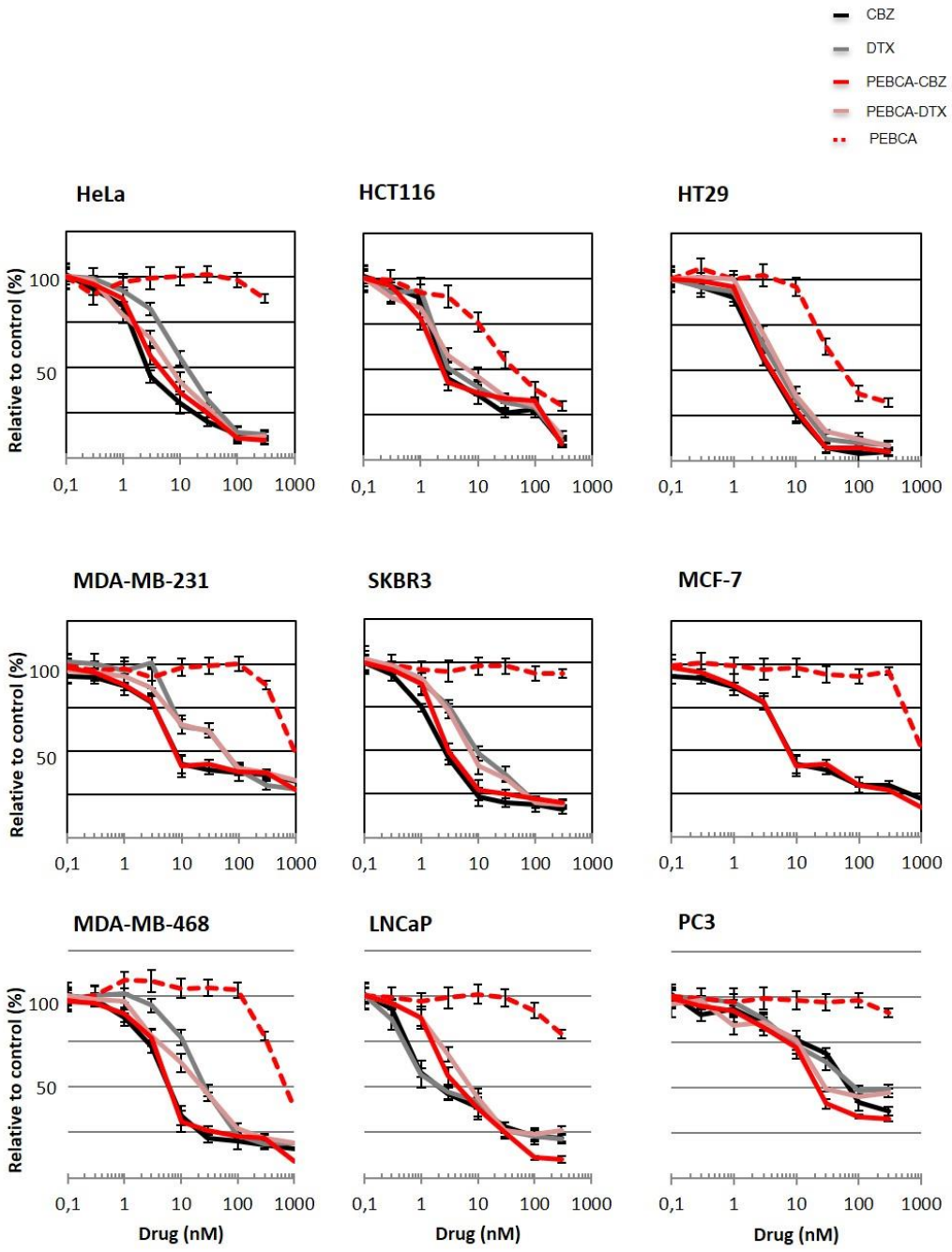

Supplementary Figure 4. Comparison of the toxic effect obtained with the MTT assay after 72 h incubation with CBZ, DTX, PEBCA-CBZ, PEBCA-DTX and empty PEBCA on the nine cell lines. The colors used for free CBZ (black), PEBCA-CBZ (non-broken red) and PEBCA (broken red) are as used in all other figures. Free DTX (grey) and PEBCA-DTX (rose). The mean values ± SEM from three independent experiments are shown.

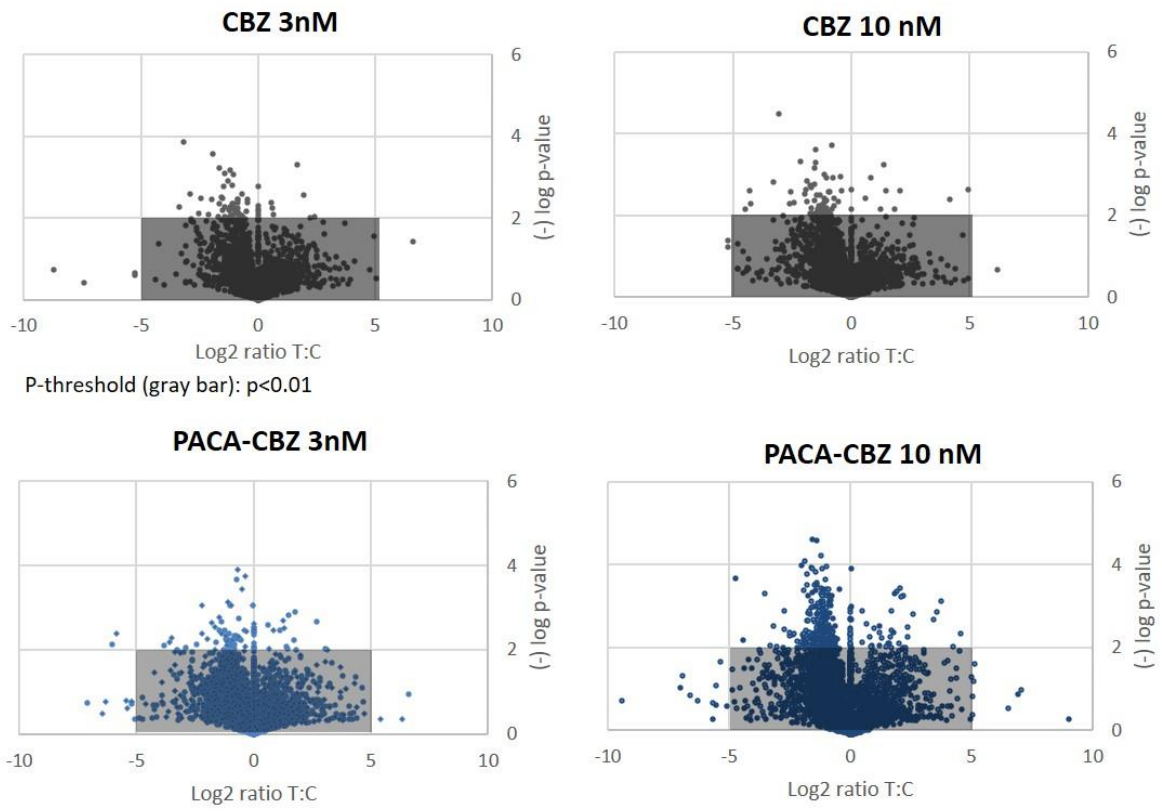

Supplementary Figure 5. Volcano plots. Protein hits for each treatment in HCT116 cells compared to untreated cells and displayed with significance threshold (log p-value Fisher exact test) and protein (LFQ) abundance (-log2 ratio). Grey area indicates proteins below threshold for significance and abundance ratio and covers proteins expected to be of little interest. The two plots on the top were obtained following incubation of cells with 3 or 10 nM CBZ. The two plots at the bottom were obtained following incubation of cells with the three types of PACA particles (PEBCA, PBCA and POCA) containing either 3 or 10 nM CBZ and then combining the data obtained for the three CBZ-containing PACAs at each CBZ concentration.

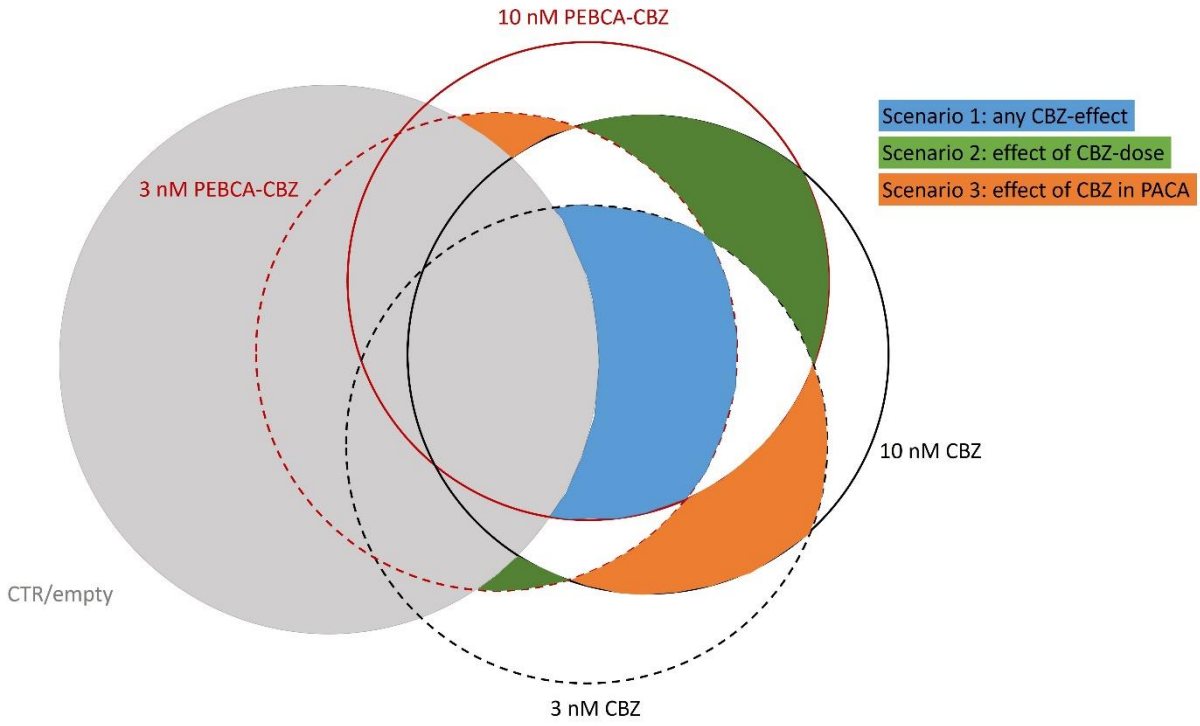

Supplementary Figure 6. A Venn diagram describing the relationship between scenarios investigated in this study. Each circle depicts the altered protein population found for each treatment. Overlap means no significant change between protein populations. Scenarios 1, 2 and 3 are illustrated as colored areas. Area sizes do not reflect number of proteins. CTR/empty: Untreated cells and cells treated with empty PACAs.

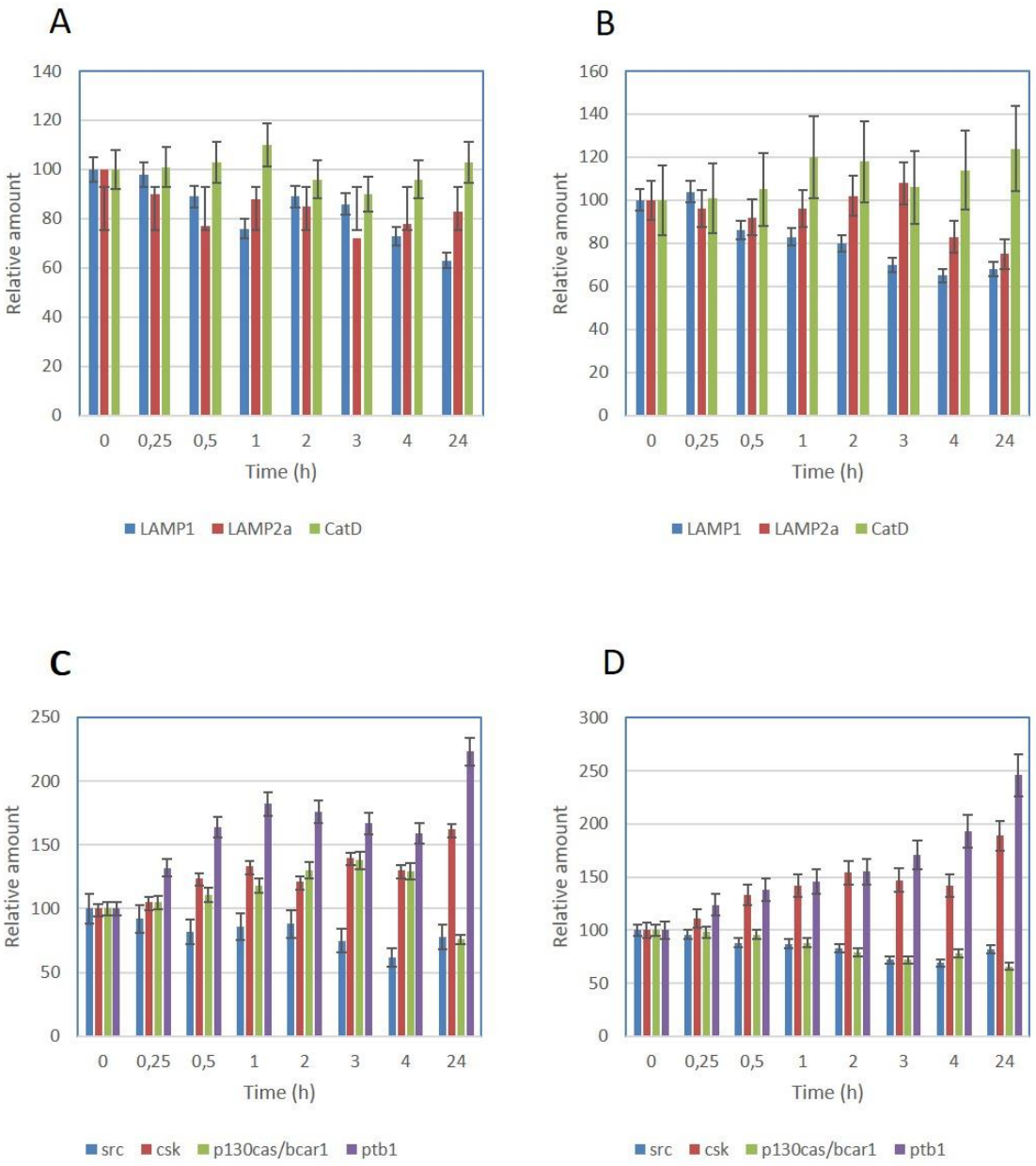

Supplementary Figure 7. Western blotting of HCT116 cell lysates following incubation of cells with 10 nM free CBZ or 10 nM PEBCA-CBZ for 0.25 - 24 h. Time-dependent changes of the lysosomal markers LAMP1, LAMP2a and cathepsin D obtained following incubation with free CBZ (A) or PEBCA-CBZ (B). Similar analyses were performed on the same samples with immunoblotting against SRC-pathway proteins SRC, CSK, BCAR1 and PTPB1 following treatment of cells with free CBZ (C) or PEBCA-CBZ (D). The data obtained were normalized to the protein expression of vimentin in each sample; all bars show the mean values + SEM for three independent experiments.

Supplementary Table 1. Listing of all proteins showing changes following the treatments described as Scenario 1,2 or 3 in Table 2 (data shown in Figure 5, 6 and 7) for HCT116 cells. Proteins hits with increased ratios between tested comparisons are shown in blue and proteins hits with decreased ratios are shown in red. The intensity of the color increases with increasing effects. Only significant hits (p-value<0.01) shown. These data are also attached as an Excel file where the data can be extracted for further use. INF=infinite - indicate that the protein was not detected in control samples. 0 - indicate that the protein was not detected in treated samples. p-value indicate significance denoted by Fisher's Exact test. Note that the alpha-2-macroglobulin hit most likely is caused by the fetal calf serum in the culture medium.

The Excel fil where the data can be extracted for further use will be added after acceptance of the manuscript.

Supplementary table 1 (HCT116)			HCT116					
			Ctr vs CBZ all		CBZ high vs CBZ low		PACA-CBZ vs free	
Protein names	Uniprot Entry	Gene names	Ratio	p-value	Ratio	<0.001	Ratio	p-value
14-3-3 protein gamma (Protein kinase C inhibitor protein 1) (KCIP-1) [Cleaved into: 14-3-3 protein gamma, N-terminally processed]	P61981	YWHAG					0.87	<0.001
14-3-3 protein zeta/delta (Protein kinase C inhibitor protein 1) (KCIP-1)	P63104	YWHAZ	1.44	<0.001				
28S ribosomal protein S23, mitochondrial (MRP-S23) (S23mt) (Mitochondrial small ribosomal subunit protein mS23)	Q9Y3D9	MRPS23					0.85	<0.001
40S ribosomal protein S11 (Small ribosomal subunit protein uS17)	P62280	RPS11	0.64	<0.001				
40S ribosomal protein S13 (Small ribosomal subunit protein uS15)	P62277	RPS13			0.8	<0.001		
40S ribosomal protein S21 (Small ribosomal subunit protein eS21)	P63220	RPS21					0.92	<0.001
40S ribosomal protein S23 (Small ribosomal subunit protein uS12)	P62266	RPS23			0.83	<0.001		
40S ribosomal protein S24 (Small ribosomal subunit protein eS24)	P62847	RPS24	0.64	<0.001				
40S ribosomal protein S28 (Small ribosomal subunit protein eS28)	P62857	ZNF428					0.76	<0.001
40S ribosomal protein S3 (EC 4.2.99.18) (Small ribosomal subunit protein uS3)	P23396	RPS3			0.89	<0.001		
40S ribosomal protein S5 (Small ribosomal subunit protein uS7) [Cleaved into: 40S ribosomal protein S5, N-terminally processed]	P46782	RPS5			0.8	<0.001		
5'-nucleotidase domain-containing protein 1 (EC 3.1.3.-)	Q5TFE4	NT5DC1			2.38	<0.001		
60 kDa SS-A/Ro ribonucleoprotein (60 kDa Ro protein) (60 kDa ribonucleoprotein Ro) (Ro60) (RoRNP) (Ro 60 kDa autoantigen) (Ro60	P10155	TROVE2					1.15	<0.001
60S acidic ribosomal protein P2 (Large ribosomal subunit protein P2) (Renal carcinoma antigen NY-REN-44)	P05387	RPLP2			1.32	<0.001		
60S ribosomal protein L10 (Laminin receptor homolog) (Large ribosomal subunit protein uL16) (Protein QM) (Ribosomal protein L10)	P27635	RPL10					0.87	<0.001
60S ribosomal protein L11 (CLL-associated antigen KW-12) (Large ribosomal subunit protein uL5)	P62913	RPL11			0.84	<0.001		
60S ribosomal protein L13 (Breast basic conserved protein 1) (Large ribosomal subunit protein eL13)	P26373	RPL13					0.91	<0.001
60S ribosomal protein L26 (Large ribosomal subunit protein uL24)	P61254	RPL26	0.64	<0.001				
60S ribosomal protein L27 (Large ribosomal subunit protein eL27)	P61353	RPL27	0.65	<0.001				
60S ribosomal protein L28 (Large ribosomal subunit protein eL28)	P46779	RPL28					0.9	<0.001
60S ribosomal protein L29 (Cell surface heparin-binding protein HIP) (Large ribosomal subunit protein eL29)	P47914	MYDGF					0.74	<0.001
60S ribosomal protein L31 (Large ribosomal subunit protein eL31)	P62899	CPT1A			0.68	<0.001		
60S ribosomal protein L32 (Large ribosomal subunit protein eL32)	P62910	RPL32	0.55	<0.001			1.05	<0.001
60S ribosomal protein L34 (Large ribosomal subunit protein eL34)	P49207	RPL34	0.71	<0.001				
60S ribosomal protein L36a (60S ribosomal protein L44) (Cell growth-inhibiting gene 15 protein) (Cell migration-inducing gene 6 prote	P83881	RPL36A			0.82	<0.001		
60S ribosomal protein L38 (Large ribosomal subunit protein eL38)	P63173	RPL38	0.65	<0.001				
60S ribosomal protein L4 (60S ribosomal protein L1) (Large ribosomal subunit protein uL4)	P36578	RPL4	0.62	<0.001				
60S ribosomal protein L7a (Large ribosomal subunit protein eL8) (PLA-X polypeptide) (Surfeit locus protein 3)	P62424	RPL7A	0.74	<0.001				
60S ribosomal protein L8 (Large ribosomal subunit protein uL2)	P62917	RPL8					0.85	<0.001
Actin-related protein 2/3 complex subunit 1B (Arp2/3 complex 41 kDa subunit) (p41-ARC)	O15143	AHNAK			1.2	<0.001		
Alpha-actinin-4 (Non-muscle alpha-actinin 4)	O43707	ACTN4			1.15	<0.001		
Annexin A2 (Annexin II) (Annexin-2) (Calpactin I heavy chain) (Calpactin-1 heavy chain) (Chromobindin-8) (Lipocortin II) (Placental an	P07355	ANXA2	1.18	<0.001				
Annexin A5 (Anchorin CII) (Annexin V) (Annexin-5) (Calphobindin I) (CBP-I) (Endonexin II) (Lipocortin V) (Placental anticoagulant prote	P08758	ANXA5	1.43	<0.001				
Apolipoprotein B-100 (Apo B-100) [Cleaved into: Apolipoprotein B-48 (Apo B-48)]	P04114	METAP1			1.19	<0.001		
Apolipoprotein C-III (Apo-CIII) (ApoC-III) (Apolipoprotein C3)	P02656	APOC3					0.44	<0.001
Ataxin-10 (Brain protein E46 homolog) (Spinocerebellar ataxia type 10 protein)	Q9UBB4	ATXN10					1.07	<0.001
Ataxin-2-like protein (Ataxin-2 domain protein) (Ataxin-2-related protein)	Q8WWM7	ATXN2L					0.84	<0.001
Barrier-to-autointegration factor (Breakpoint cluster region protein 1) [Cleaved into: Barrier-to-autointegration factor, N-terminally p	O75531	EIF2S1			1.26	<0.001		
Bcl-2-associated transcription factor 1 (Btf) (BCLAF1 and THRAP3 family member 1)	Q9NYF8	BCLAF1			0.82	<0.001		
Brain-specific angiogenesis inhibitor 1-associated protein 2 (BAI-associated protein 2) (BAI1-associated protein 2) (Protein BAP2) (Fas	Q9UQB8	BAIAP2	0.52	<0.001				
Bystin	Q13895	PRRC2C			0.64	<0.001		
Calponin-2 (Calponin H2, smooth muscle) (Neutral calponin)	Q99439	CNN2					0.89	<0.001
Calponin-3 (Calponin, acidic isoform)	Q15417	CNN3	0.52	<0.001	1.21	<0.001		
Carnitine O-palmitoyltransferase 1, liver isoform (CPT1-L) (EC 2.3.1.21) (Carnitine O-palmitoyltransferase I, liver isoform) (CPT I) (CPTI-	P50416	SLC7A5			0.69	<0.001		
Catalase (EC 1.11.1.6)	P04040	CAT					0.79	<0.001
CD9 antigen (5H9 antigen) (Cell growth-inhibiting gene 2 protein) (Leukocyte antigen MIC3) (Motility-related protein) (MRP-1) (Tetra	P21926	CD9					1.18	<0.001
Cell division control protein 42 homolog (EC 3.6.5.2) (G25K GTP-binding protein)	P60953	CDC42					1.27	<0.001
Cellular nucleic acid-binding protein (CNBP) (Zinc finger protein 9)	P62633	CNBP			0.77	<0.001		
Chloride intracellular channel protein 4 (Intracellular chloride ion channel protein p64H1)	Q9Y696	CLIC4			0.78	<0.001		
Cleavage and polyadenylation specificity factor subunit 6 (Cleavage and polyadenylation specificity factor 68 kDa subunit) (CPSF 68 k	Q16630	CPSF6					0.86	<0.001
Clustered mitochondria protein homolog	O75153	CLUH			1.56	<0.001		
Coiled-coil domain-containing protein 86 (Cytokine-induced protein with coiled-coil domain)	Q9H6F5	NPM3					0.77	<0.001
Cold-inducible RNA-binding protein (A18 hnRNP) (Glycine-rich RNA-binding protein CIRP)	Q14011	CIRBP			0.78	<0.001		
Collagen alpha-2(I) chain (Alpha-2 type I collagen)	P08123	COL1A2			1.4	<0.001		

			Ctr vs CBZ all		CBZ high vs CBZ low		PACA-CBZ vs free	
Protein names	Uniprot Entry	Gene names	Ratio	p-value	Ratio	<0.001	Ratio	p-value
Complement component 1 Q subcomponent-binding protein, mitochondrial (ASF/SF2-associated protein p32) (Glycoprotein gC1qBP	Q07021	C1QBP	3.49	<0.001				
Coronin-1B (Coronin-2)	Q9BR76	CORO1B			1.15	<0.001		
Cyclin-dependent kinase 1 (CDK1) (EC 2.7.11.22) (EC 2.7.11.23) (Cell division control protein 2 homolog) (Cell division protein kinase	P06493	CDK1			0.86	<0.001		
CYFIP-related Rac1 interactor B (L1)	Q9NUQ9	FAM49B			0.83	<0.001		
Cytochrome c oxidase subunit 7A2, mitochondrial (Cytochrome c oxidase subunit VIIa-liver/heart) (Cytochrome c oxidase subunit VII	P14406	COX7A2			0	<0.001		
DAZ-associated protein 1 (Deleted in azoospermia-associated protein 1)	Q96EP5	DAZAP1					0.7	<0.001
Destrin (Actin-depolymerizing factor) (ADF)	P60981	DSTN			1.49	<0.001		
Dihydropteridine reductase (EC 1.5.1.34) (HDHPR) (Quinoid dihydropteridine reductase) (Short chain dehydrogenase/reductase fami	P09417	QDPR	0.50	<0.001				
DNA (cytosine-5)-methyltransferase 1 (Dnmt1) (EC 2.1.1.37) (CXXC-type zinc finger protein 9) (DNA methyltransferase HsaI) (DNA MTa	P26358	DNMT1					3.28	<0.001
DNA repair protein complementing XP-C cells (Xeroderma pigmentosum group C-complementing protein) (p125)	Q01831	XPC					1.25	<0.001
DnaJ homolog subfamily B member 1 (DnaJ protein homolog 1) (Heat shock 40 kDa protein 1) (HSP40) (Heat shock protein 40) (Huma	P25685	DNAJB1			0.82	<0.001		
DnaJ homolog subfamily C member 2 (M-phase phosphoprotein 11) (Zuotin-related factor 1) [Cleaved into: DnaJ homolog subfamily	Q99543	DNAJC2			0.16	<0.001		
DnaJ homolog subfamily C member 8 (Splicing protein spf31)	O75937	DNAJC8	5.45	<0.001				
Elongation factor 1-alpha 1 (EF-1-alpha-1) (Elongation factor Tu) (EF-Tu) (Eukaryotic elongation factor 1 A-1) (eEF1A-1) (Leukocyte rec	P68104	EEF1A1			1.15	<0.001		
Elongation factor 1-beta (EF-1-beta)	P24534	LGALS3			1.25	<0.001		
Epithelial splicing regulatory protein 1 (RNA-binding motif protein 35A) (RNA-binding protein 35A)	Q6NXG1	RAB10			0.51	<0.001		
Ethylmalonyl-CoA decarboxylase (EC 4.1.1.94) (Enoyl-CoA hydratase domain-containing protein 1) (Methylmalonyl-CoA decarboxyla	Q9NTX5	ECHDC1					1.27	<0.001
Eukaryotic translation initiation factor 1A, X-chromosomal (eIF-1A X isoform) (Eukaryotic translation initiation factor 4C) (eIF-4C)	P47813	EIF1AX			1.31	<0.001		
Eukaryotic translation initiation factor 2 subunit 1 (Eukaryotic translation initiation factor 2 subunit alpha) (eIF-2-alpha) (eIF-2A) (eIF-	P05198	RCC1			1.26	<0.001		
Eukaryotic translation initiation factor 4H (eIF-4H) (Williams-Beuren syndrome chromosomal region 1 protein)	Q15056	EIF4H					1.13	<0.001
Eukaryotic translation initiation factor 5A-1 (eIF-5A-1) (eIF-5A1) (Eukaryotic initiation factor 5A isoform 1) (eIF-5A) (Rev-binding factor	P63241	EIF5A			1.33	<0.001		
Exportin-1 (Exp1) (Chromosome region maintenance 1 protein homolog)	O14980	XPO1			1.39	<0.001		
Exportin-2 (Exp2) (Cellular apoptosis susceptibility protein) (Chromosome segregation 1-like protein) (Importin-alpha re-exporter)	P55060	CSE1L					1.35	<0.001
Ezrin (Cytovillin) (Villin-2) (p81)	P15311	EZR					0.91	<0.001
Fatty acid-binding protein 5 (Epidermal-type fatty acid-binding protein) (E-FABP) (Fatty acid-binding protein, epidermal) (Psoriasis-as	Q01469	NAP1L1			1.18	<0.001		
Galectin-3 (Gal-3) (35 kDa lectin) (Carbohydrate-binding protein 35) (CBP 35) (Galactose-specific lectin 3) (Galactoside-binding protei	P17931	CNN3			1.24	<0.001		
Glucose-6-phosphate isomerase (GPI) (EC 5.3.1.9) (Autocrine motility factor) (AMF) (Neuroleukin) (NLK) (Phosphoglucose isomerase)	P06744	GPI			1.11	<0.001		
Glutaminase kidney isoform, mitochondrial (GLS) (EC 3.5.1.2) (K-glutaminase) (L-glutamine amidohydrolase) [Cleaved into: Glutamin	O94925	SEC61B			0.47	<0.001		
Glutathione S-transferase omega-1 (GSTO-1) (EC 2.5.1.18) (Glutathione S-transferase omega 1-1) (GSTO 1-1) (Glutathione-dependent	P78417	GSTO1			1.14	<0.001		
Glyceraldehyde-3-phosphate dehydrogenase (GAPDH) (EC 1.2.1.12) (Peptidyl-cysteine S-nitrosylase GAPDH) (EC 2.6.99.-)	P04406	GAPDH			1.1	<0.001		
Glycine N-acyltransferase (EC 2.3.1.13) (Acyl-CoA:glycine N-acyltransferase) (AAc) (Aralkyl acyl-CoA N-acyltransferase) (Aralkyl acyl-Co	Q6IB77	SEC23IP					0.78	<0.001
Glycine--tRNA ligase (EC 6.1.1.14) (Diadenosine tetraphosphate synthetase) (Ap4A synthetase) (EC 2.7.7.-) (Glycyl-tRNA synthetase) (	P41250	GARS					0.87	<0.001
Growth/differentiation factor 15 (GDF-15) (Macrophage inhibitory cytokine 1) (MIC-1) (NSAID-activated gene 1 protein) (NAG-1) (NSA	Q99988	GDF15	2.66	<0.001				
Growth/differentiation factor 15 (GDF-15) (Macrophage inhibitory cytokine 1) (MIC-1) (NSAID-activated gene 1 protein) (NAG-1) (NSA	Q99988	GDF15					0.71	<0.001
GTPase KRas (K-Ras 2) (Ki-Ras) (c-K-ras) (c-Ki-ras) [Cleaved into: GTPase KRas, N-terminally processed]	P01116	KRAS			0	<0.001		
Guanine nucleotide-binding protein-like 1 (GTP-binding protein HSR1)	P36915	GNL1	0.52	<0.001				
Heat shock protein beta-1 (HspB1) (28 kDa heat shock protein) (Estrogen-regulated 24 kDa protein) (Heat shock 27 kDa protein) (HSP	P04792	HSPB1					0.93	<0.001
Heterogeneous nuclear ribonucleoprotein D0 (hnRNP D0) (AU-rich element RNA-binding protein 1)	Q14103	HNRNPD			1.14	<0.001		
Heterogeneous nuclear ribonucleoproteins A2/B1 (hnRNP A2/B1)	P22626	HNRNPA2B1					0.88	<0.001
Histone deacetylase 2 (HD2) (EC 3.5.1.98)	Q92769	HDAC2					0.87	<0.001
Histone H1.4 (Histone H1b) (Histone H1s-4)	P10412	HIST1H1A					0.92	<0.001
Histone H2A.V (H2A.F/Z) (H2A.Z variant histone 2)	Q71UI9	H2AFV	0.59	<0.001				
Histone H2B type 2-E (H2B-clustered histone 21) (Histone H2B-GL105) (Histone H2B.q) (H2B/q)	Q16778	HIST2H2BE	0.50	<0.001				
Host cell factor 1 (HCF) (HCF-1) (C1 factor) (CFF) (VCAF) (VP16 accessory protein) [Cleaved into: HCF N-terminal chain 1; HCF N-termin	P51610	HCFC1	0.61	<0.001				
Hsc70-interacting protein (Hip) (Aging-associated protein 2) (Progesterone receptor-associated p48 protein) (Protein FAM10A1) (Puta	P50502	ST13			1.13	<0.001		
Importin subunit alpha-1 (Karyopherin subunit alpha-2) (RAG cohort protein 1) (SRP1-alpha)	P52292	KPNA2			0.85	<0.001		
Interleukin enhancer-binding factor 3 (Double-stranded RNA-binding protein 76) (DRBP76) (M-phase phosphoprotein 4) (MPP4) (Nuc	Q12906	ILF3	0.73	<0.001	1.21	<0.001		
Keratin, type I cytoskeletal 19 (Cytokeratin-19) (CK-19) (Keratin-19) (K19)	P08727	KRT19					1.28	<0.001
Keratin, type II cytoskeletal 8 (Cytokeratin-8) (CK-8) (Keratin-8) (K8) (Type-II keratin Kb8)	P05787	KRT8			1.21	<0.001	1.29	<0.001
La-related protein 4B (La ribonucleoprotein domain family member 4B) (La ribonucleoprotein domain family member 5) (La-related p	Q92615	AATF			0.53	<0.001		
Large neutral amino acids transporter small subunit 1 (4F2 light chain) (4F2 LC) (4F2LC) (CD98 light chain) (Integral membrane protein	Q01650	NXF1			0.72	<0.001		
Leucine-rich repeat-containing protein 47	Q8N1G4	LRRC47			0.82	<0.001		
Lupus La protein (La autoantigen) (La ribonucleoprotein) (Sjoegren syndrome type B antigen) (SS-B)	P05455	SSB					0.9	<0.001
L-xylulose reductase (XR) (EC 1.1.1.10) (Carbonyl reductase II) (Dicarbonyl/L-xylulose reductase) (Kidney dicarbonyl reductase) (kiDCR	Q7Z4W1	DCXR	0.58	<0.001				
Lysosome-associated membrane glycoprotein 1 (LAMP-1) (Lysosome-associated membrane protein 1) (CD107 antigen-like family mem	P11279	LAMP1	0.07	<0.001				
Malignant T-cell-amplified sequence 1 (MCT-1) (Multiple copies T-cell malignancies)	Q9ULC4	MCTS1			2.62	<0.001		

			Ctr vs CBZ all		CBZ high vs CBZ low		PACA-CBZ vs free	
Protein names	Uniprot Entry	Gene names	Ratio	p-value	Ratio	<0.001	Ratio	p-value
MARCKS-related protein (MARCKS-like protein 1) (Macrophage myristoylated alanine-rich C kinase substrate) (Mac-MARCKS) (MacM	P49006	MARCKSL1	INF	<0.001				
Matrin-3	P43243	MATR3			1.08	<0.001		
Metallothionein-1X (MT-1X) (Metallothionein-IX) (MT-IX)	P80297	HIST2H3A			0.72	<0.001		
Methionine aminopeptidase 1 (MAP 1) (MetAP 1) (EC 3.4.11.18) (Peptidase M 1)	P53582	PTGES3			1.18	<0.001		
Methylosome protein 50 (MEP-50) (Androgen receptor cofactor p44) (WD repeat-containing protein 77) (p44/Mep50)	Q9BQA1	WDR77	9.98	<0.001				
Mitochondrial tRNA-specific 2-thiouridylase 1 (EC 2.8.1.14) (MTO2 homolog)	O75648	NOM1			0.39	<0.001		
Mitotic interactor and substrate of PLK1 (Mitotic spindle positioning protein)	Q8IVT2	MISP	0.57	<0.001				
Myeloid-derived growth factor (MYDGF)	Q969H8	HIST1H2B					0.72	<0.001
Nascent polypeptide-associated complex subunit alpha (NAC-alpha) (Alpha-NAC) (allergen Hom s 2)	Q13765	BANF1			1.27	<0.001		
Nascent polypeptide-associated complex subunit alpha, muscle-specific form (Alpha-NAC, muscle-specific form) (skNAC)	E9PAV3	NACA			1.3	<0.001		
Neuroblast differentiation-associated protein AHNAK (Desmoyokin)	Q09666	APOB			1.2	<0.001		
Nicotinamide phosphoribosyltransferase (NAmPRTase) (Nampt) (EC 2.4.2.12) (Pre-B-cell colony-enhancing factor 1) (Pre-B cell-enhan	P43490	NAMPT			1.16	<0.001		
Nuclear RNA export factor 1 (Tip-associated protein) (Tip-associating protein) (mRNA export factor TAP)	Q9UBU9	MT1X			0.72	<0.001		
Nucleobindin-1 (CALNUC)	Q02818	UBE2C			0.45	<0.001		
Nucleolar MIF4G domain-containing protein 1 (SGD1 homolog)	Q5C9Z4	NOM1			0.4	<0.001	2.2	<0.001
Nucleolar protein 3 (Apoptosis repressor with CARD) (Muscle-enriched cytoplasmic protein) (Myp) (Nucleolar protein of 30 kDa) (Nop	O60936	NOL3			0	<0.001		
Nucleolin (Protein C23)	P19338	NCL	1.34	<0.001	1.12	<0.001		
Nucleoplasmin-3	O75607	RPS28					0.77	<0.001
Nucleosome assembly protein 1-like 1 (NAP-1-related protein) (hNRP)	P55209	PRDX1			1.18	<0.001		
Obg-like ATPase 1 (DNA damage-regulated overexpressed in cancer 45) (DOC45) (GTP-binding protein 9)	Q9NTK5	OLA1					1.23	<0.001
Pantetheinase (EC 3.5.1.92) (Pantetheine hydrolase) (Tiff66) (Vascular non-inflammatory molecule 1) (Vanin-1)	O95497	VNN1			1.38	<0.001		
Paxillin	P49023	PXN					0.83	<0.001
PDZ and LIM domain protein 7 (LIM mineralization protein) (LMP) (Protein enigma)	Q9NR12	PDLIM7	0.65	<0.001			0.84	<0.001
Perilipin-3 (47 kDa mannose 6-phosphate receptor-binding protein) (47 kDa MPR-binding protein) (Cargo selection protein TIP47) (M	O60664	PLIN3			1.16	<0.001		
Peroxiredoxin-1 (EC 1.11.1.15) (Natural killer cell-enhancing factor A) (NKEF-A) (Proliferation-associated gene protein) (PAG) (Thiored	Q06830	TUBB2A			1.18	<0.001		
Phosphoglycerate kinase 1 (EC 2.7.2.3) (Cell migration-inducing gene 10 protein) (Primer recognition protein 2) (PRP 2)	P00558	PGK1			1.14	<0.001		
Phosphoserine phosphatase (PSP) (PSPase) (EC 3.1.3.3) (L-3-phosphoserine phosphatase) (O-phosphoserine phosphohydrolase)	P78330	PSPH					0.47	<0.001
PIH1 domain-containing protein 1 (Nucleolar protein 17 homolog)	Q9NWS0	PIH1D1			5.87	<0.001		
Plasminogen activator inhibitor 1 RNA-binding protein (PAI1 RNA-binding protein 1) (PAI-RBP1) (SERPINE1 mRNA-binding protein 1)	Q8NC51	SERBP1			0.78	<0.001		
Poly(U)-binding-splicing factor PUF60 (60 kDa poly(U)-binding-splicing factor) (FUSE-binding protein-interacting repressor) (FBP-intera	Q9UHX1	PUF60			1.13	<0.001		
Polyglutamine-binding protein 1 (PQBP-1) (38 kDa nuclear protein containing a WW domain) (Npw38) (Polyglutamine tract-binding p	O60828	PQBP1					0.92	<0.001
Prefoldin subunit 6 (Protein Ke2)	O15212	CCDC86					0.78	<0.001
Pre-mRNA-processing factor 19 (EC 2.3.2.27) (Nuclear matrix protein 200) (PRP19/PSO4 homolog) (hPso4) (RING-type E3 ubiquitin tra	Q9UMS4	PRPF19			1.15	<0.001		
Pre-mRNA-splicing regulator WTAP (Female-lethal(2)D homolog) (hFL(2)D) (WT1-associated protein) (Wilms tumor 1-associating prot	Q15007	RPL29					0.76	<0.001
pre-rRNA 2'-O-ribose RNA methyltransferase FTSJ3 (EC 2.1.1.-) (Protein ftsJ homolog 3) (Putative rRNA methyltransferase 3)	Q8IY81	FTSJ3			0.83	<0.001		
PRKC apoptosis WT1 regulator protein (Prostate apoptosis response 4 protein) (Par-4)	Q96IZ0	NUCB1			0.4	<0.001		
Probable ATP-dependent RNA helicase DDX27 (EC 3.6.4.13) (DEAD box protein 27)	Q96GQ7	DDX27			0.85	<0.001		
Probable ATP-dependent RNA helicase DDX56 (EC 3.6.4.13) (ATP-dependent 61 kDa nucleolar RNA helicase) (DEAD box protein 21) (D	Q9NY93	DDX56					0.7	<0.001
Probable ATP-dependent RNA helicase DDX6 (EC 3.6.4.13) (ATP-dependent RNA helicase p54) (DEAD box protein 6) (Oncogene RCK)	P26196	DDX6			1.15	<0.001		
Probable rRNA-processing protein EBP2 (EBNA1-binding protein 2) (Nucleolar protein p40)	Q99848	EBNA1BP2					0.71	<0.001
Profilin-1 (Epididymis tissue protein Li 184a) (Profilin I)	P07737	PFN1					0.97	<0.001
Profilin-2 (Profilin II)	P35080	PFN2					0.82	<0.001
Prostaglandin E synthase 3 (EC 5.3.99.3) (Cytosolic prostaglandin E2 synthase) (cPGES) (Hsp90 co-chaperone) (Progesterone receptor	Q15185	FABP5			1.18	<0.001		
Proteasome assembly chaperone 1 (PAC-1) (Chromosome 21 leucine-rich protein) (C21-LRP) (Down syndrome critical region protein 2	O95456	PSMG1			1.4	<0.001		
Proteasome subunit alpha type-4 (EC 3.4.25.1) (Macropain subunit C9) (Multicatalytic endopeptidase complex subunit C9) (Proteaso	P25789	PSMA4			1.16	<0.001		
Protein AATF (Apoptosis-antagonizing transcription factor) (Rb-binding protein Che-1)	Q9NY61	WDR74			0.59	<0.001		
Protein ABHD14B (EC 3.-.-.-) (Alpha/beta hydrolase domain-containing protein 14B) (Abhydrolase domain-containing protein 14B) (C	Q96IU4	ABHD14B			0.75	<0.001		
Protein arginine N-methyltransferase 1 (EC 2.1.1.319) (Histone-arginine N-methyltransferase PRMT1) (Interferon receptor 1-bound pr	Q99873	PRMT1			1.2	<0.001	1.3	<0.001
Protein FAM136A	Q96C01	FAM136A					0.46	<0.001
Protein LSM12 homolog	Q3MHD2	LSM12					0.81	<0.001
Protein PRRC2A (HLA-B-associated transcript 2) (Large proline-rich protein BAT2) (Proline-rich and coiled-coil-containing protein 2A) (	P48634	PRRC2A					0.7	<0.001
Protein PRRC2C (BAT2 domain-containing protein 1) (HBV X-transactivated gene 2 protein) (HBV XAg-transactivated protein 2) (HLA-B	Q9Y520	RBM28			0.68	<0.001		
Protein RRP5 homolog (NF-kappa-B-binding protein) (NFBP) (Programmed cell death protein 11)	Q14690	PDCD11			0.76	<0.001		
Protein transport protein Sec24C (SEC24-related protein C)	P53992	SEC24C			0.19	<0.001		
Protein transport protein Sec61 subunit beta	P60468	ESRP1			0.48	<0.001		
Prothymosin alpha [Cleaved into: Prothymosin alpha, N-terminally processed; Thymosin alpha-1]	P06454	PTMA	2.82	<0.001				

			Ctr vs CBZ all		CBZ high vs CBZ low		PACA-CBZ vs free	
Protein names	Uniprot Entry	Gene names	Ratio	p-value	Ratio	<0.001	Ratio	p-value
Proto-oncogene tyrosine-protein kinase Src (EC 2.7.10.2) (Proto-oncogene c-Src) (pp60c-src) (p60-Src)	P12931	SRC					0.67	<0.001
Putative heat shock protein HSP 90-beta 2 (Heat shock protein 90-beta b) (Heat shock protein 90Bb)	Q58FF8	HSP90AB2P					1.31	<0.001
Pyrroline-5-carboxylate reductase 2 (P5C reductase 2) (P5CR 2) (EC 1.5.1.2)	Q96C36	PYCR2			0.72	<0.001		
Ras GTPase-activating protein-binding protein 2 (G3BP-2) (GAP SH3 domain-binding protein 2)	Q9UN86	G3BP2			1.37	<0.001		
Ras-related protein Rab-10 (EC 3.6.5.2)	P61026	LARP4B			0.52	<0.001		
Ras-related protein Rab-1A (YPT1-related protein)	P62820	RAB1A					1.52	<0.001
Regulator of chromosome condensation (Cell cycle regulatory protein) (Chromosome condensation protein 1)	P18754	EEF1B2			1.25	<0.001		
Rho GDP-dissociation inhibitor 1 (Rho GDI 1) (Rho-GDI alpha)	P52565	ARHGDIA					1.1	<0.001
Ribosomal RNA small subunit methyltransferase NEP1 (EC 2.1.1.-) (18S rRNA (pseudouridine(1248)-N1)-methyltransferase) (18S rRNA	Q92979	EMG1			0.88	<0.001		
Ribosome biogenesis protein BMS1 homolog (Ribosome assembly protein BMS1 homolog)	Q14692	BMS1					0.87	<0.001
Ribosome biogenesis protein WDR12 (WD repeat-containing protein 12)	Q9GZL7	WDR12			1.14	<0.001		
RNA-binding protein 14 (Paraspeckle protein 2) (PSP2) (RNA-binding motif protein 14) (RRM-containing coactivator activator/modula	Q96PK6	RBM14	0.64	<0.001				
RNA-binding protein 28 (RNA-binding motif protein 28)	Q9NW13	RPL31			0.68	<0.001		
RNA-binding protein PNO1 (Partner of NOB1)	Q9NRX1	PNO1			0	<0.001		
SEC23-interacting protein (p125)	Q9Y6Y8	PFDN6					0.78	<0.001
Septin-11	Q9NVA2	SEPTIN11			1.33	<0.001		
Serine/arginine repetitive matrix protein 1 (SR-related nuclear matrix protein of 160 kDa) (SRm160) (Ser/Arg-related nuclear matrix p	Q8IYB3	SRRM1			2.81	<0.001		
Serine/arginine repetitive matrix protein 2 (300 kDa nuclear matrix antigen) (Serine/arginine-rich splicing factor-related nuclear matr	Q9UQ35	SRRM2					0.89	<0.001
Serine/threonine-protein phosphatase 2A 55 kDa regulatory subunit B alpha isoform (PP2A subunit B isoform B55-alpha) (PP2A subu	P63151	PPP2R2A	1.52	<0.001				
Small nuclear ribonucleoprotein F (snRNP-F) (Sm protein F) (Sm-F) (SmF)	P62306	SNRPF	4.79	<0.001				
Small nuclear ribonucleoprotein Sm D2 (Sm-D2) (snRNP core protein D2)	P62316	TUBB4B			1.17	<0.001		
Small nuclear ribonucleoprotein Sm D3 (Sm-D3) (snRNP core protein D3)	P62318	SNRPD3					0.82	<0.001
Small nuclear ribonucleoprotein-associated protein N (snRNP-N) (Sm protein D) (Sm-D) (Sm protein N) (Sm-N) (SmN) (Tissue-specific-	P63162	SNRPN	0.60	<0.001				
Spliceosome RNA helicase DDX39B (EC 3.6.4.13) (56 kDa U2AF65-associated protein) (ATP-dependent RNA helicase p47) (DEAD box p	Q13838	DDX39B	0.75	<0.001				
Staphylococcal nuclease domain-containing protein 1 (EC 3.1.31.1) (100 kDa coactivator) (EBNA2 coactivator p100) (Tudor domain-co	Q7KZF4	SND1			0.89	<0.001		
Succinyl-CoA:3-ketoacid coenzyme A transferase 1, mitochondrial (EC 2.8.3.5) (3-oxoacid CoA-transferase 1) (Somatic-type succinyl-C	P55809	OXCT1			INF	<0.001		
Sulfhydryl oxidase 1 (hQSOX) (EC 1.8.3.2) (Quiescin Q6)	O00391	QSOX1			4.55	<0.001		
Syntaxin-binding protein 2 (Protein unc-18 homolog 2) (Unc18-2) (Protein unc-18 homolog B) (Unc-18B)	Q15833	STXBP2					1.32	<0.001
Tax1-binding protein 3 (Glutaminase-interacting protein 3) (Tax interaction protein 1) (TIP-1) (Tax-interacting protein 1)	O14907	TAX1BP3					3.44	<0.001
T-complex protein 1 subunit beta (TCP-1-beta) (CCT-beta)	P78371	CCT2			1.09	<0.001		
T-complex protein 1 subunit epsilon (TCP-1-epsilon) (CCT-epsilon)	P48643	CCT5			1.1	<0.001		
Thioredoxin reductase 1, cytoplasmic (TR) (EC 1.8.1.9) (Gene associated with retinoic and interferon-induced mortality 12 protein) (G	Q16881	TXNRD1					0.87	<0.001
Thioredoxin-dependent peroxide reductase, mitochondrial (EC 1.11.1.15) (Antioxidant protein 1) (AOP-1) (HBC189) (Peroxiredoxin III	P30048	PRDX3					0.81	<0.001
Transforming protein RhoA (EC 3.6.5.2) (Rho cDNA clone 12) (h12)	P61586	RHOA					1.26	<0.001
Transitional endoplasmic reticulum ATPase (TER ATPase) (EC 3.6.4.6) (15S Mg(2+)-ATPase p97 subunit) (Valosin-containing protein) (	P55072	VCP	1.24	<0.001	1.1	<0.01		
Translationally-controlled tumor protein (TCTP) (Fortilin) (Histamine-releasing factor) (HRF) (p23)	P13693	TPT1			1.35	<0.001		
Treacle protein (Treacher Collins syndrome protein)	Q13428	TCOF1	0.65	<0.001				
Trifunctional enzyme subunit alpha, mitochondrial (78 kDa gastrin-binding protein) (Monolysocardiolipin acyltransferase) (EC 2.3.1.-	P40939	HADHA			1.65	<0.001		
tRNA (guanine(26)-N(2))-dimethyltransferase (EC 2.1.1.216) (tRNA 2,2-dimethylguanosine-26 methyltransferase) (tRNA(guanine-26,N	Q9NXH9	TRMT1			0.36	<0.001		
Tropomyosin alpha-3 chain (Gamma-tropomyosin) (Tropomyosin-3) (Tropomyosin-5) (hTM5)	P06753	TPM3					0.91	<0.001
Tubulin beta-2A chain (Tubulin beta class IIa)	Q13885	SNRPD2			1.17	<0.001		
Tubulin beta-3 chain (Tubulin beta-4 chain) (Tubulin beta-III)	Q13509	TUBB3			1.62	<0.001		
Tubulin beta-4B chain (Tubulin beta-2 chain) (Tubulin beta-2C chain)	P68371	NME1-NME2			1.17	<0.001		
Tubulin beta-8 chain (Tubulin beta 8 class VIII)	Q3ZCM7	TUBB8			1.51	<0.001		
Tyrosine-protein phosphatase non-receptor type 1 (EC 3.1.3.48) (Protein-tyrosine phosphatase 1B) (PTP-1B)	P18031	PTPN1			0.19	<0.001		
U1 small nuclear ribonucleoprotein 70 kDa (U1 snRNP 70 kDa) (U1-70K) (snRNP70)	P08621	SNRNp70					1.24	<0.001
U2 small nuclear ribonucleoprotein A' (U2 snRNP A')	P09661	SNRPA1			1.42	<0.001	1.23	<0.001
U2 small nuclear ribonucleoprotein B'' (U2 snRNP B'')	P08579	SNRPB2					1.94	<0.001
U6 snRNA-associated Sm-like protein LSm8	O95777	LSM8			1.47	<0.001		
Ubiquitin carboxyl-terminal hydrolase isozyme L5 (UCH-L5) (EC 3.4.19.12) (Ubiquitin C-terminal hydrolase UCH37) (Ubiquitin thioeste	Q9Y5K5	UCHL5	INF	<0.001				
Ubiquitin-conjugating enzyme E2 C (EC 2.3.2.23) ((E3-independent) E2 ubiquitin-conjugating enzyme C) (EC 2.3.2.24) (E2 ubiquitin-co	O00762	GLS			0.46	<0.001		
Ubiquitin-fold modifier-conjugating enzyme 1 (Ufm1-conjugating enzyme 1)	Q9Y3C8	UFC1					0.51	<0.001
Ubiquitin-like protein FUBI	P62861	FAU	0.43	<0.001			0.85	<0.001
UV excision repair protein RAD23 homolog B (HR23B) (hHR23B) (XP-C repair-complementing complex 58 kDa protein) (p58)	P54727	RAD23B					2.38	<0.001
V-type proton ATPase catalytic subunit A (V-ATPase subunit A) (EC 7.1.2.2) (V-ATPase 69 kDa subunit) (Vacuolar ATPase isoform VA68	P38606	ATP6V1A			1.16	<0.001		
WD repeat-containing protein 36 (T-cell activation WD repeat-containing protein) (TA-WDRP)	Q8NI36	WDR36			0.84	<0.001	0.82	<0.001
WD repeat-containing protein 43 (U3 small nucleolar RNA-associated protein 5 homolog)	Q15061	WDR43			1.16	<0.001		
WD repeat-containing protein 74 (NOP seven-associated protein 1)	Q6RFH5	BYSL			0.61	<0.001		
YTH domain-containing family protein 3	Q7Z739	YTHDF3	INF	<0.001				
Zinc finger protein 428 (Enzyme-like protein PIT13)	Q96B54	WTAP					0.76	<0.001
Zinc finger protein ZPR1 (Zinc finger protein 259)	O75312	ZPR1			0	<0.001		
Zyxin (Zyxin-2)	Q15942	ZYX					0.88	<0.001